KERNFORSCHUNGSANLAGE JÜLICH GmbH
Zentrallabor für Elektronik
Zentralinstitut für Angewandte Mathematik

Measurement of transient magnetic fields and of eddy current time constans in TEXTOR

by

Hp. Eulenberg
H. Thyssen
B. Steffen

Jül - 1816
translation June 1984
ISSN 0366 - 0885

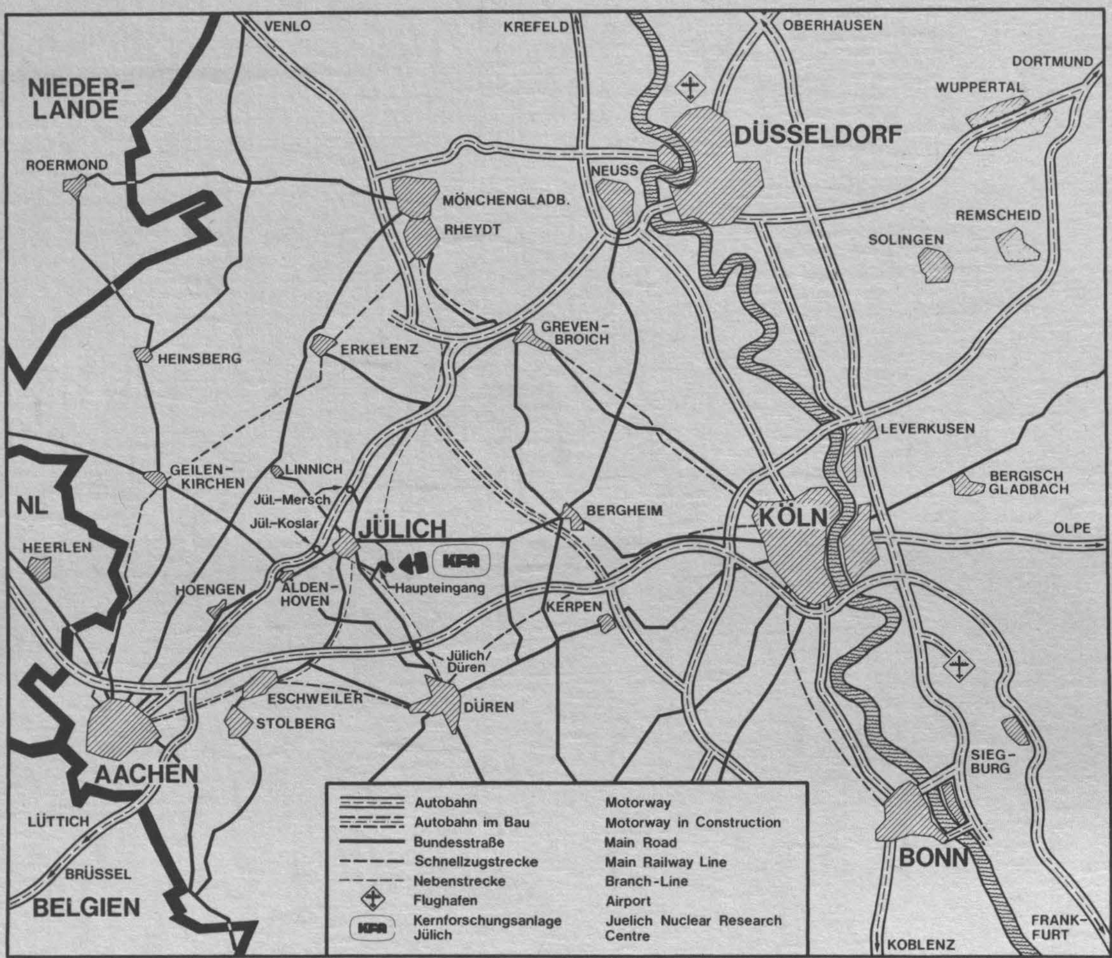

Als Manuskript gedruckt

Berichte der Kernforschungsanlage Jülich – Nr. 1816 (translation)

Zentrallabor für Elektronik – Zentralinstitut für Angewandte Mathematik Jül – 1816 (translation)

Zu beziehen durch: ZENTRALBIBLIOTHEK der Kernforschungsanlage Jülich GmbH
Postfach 1913 · D-5170 Jülich (Bundesrepublik Deutschland)
Telefon: (0 24 61) 610 · Telex: 8 33 556 kfa d

Measurement of transient magnetic fields and of eddy current time constans in TEXTOR

by

Hp. Eulenberg
H. Thyssen
B. Steffen

translated by
M. Heinz

Preface

The General Electronics Division of the Central Electronics Laboratory of the Jülich Nuclear Research Centre (KFA-ZEL) has taken over the task of measuring the position- and time-dependent magnetic fields as well as their eddy current effects in the TEXTOR Tokamak machine in cooperation with the Institute of Plasma Physics.

The measurement work was already completed after only nine days owing to the automated mode of operation of the computer-controlled measuring equipment for large-area measurement of the magnetic fields occurring every five minutes for approximately 3 seconds.

On the other hand, extensive work was required for the design and construction of the measuring machine and for the development of the measuring procedure adapted to the properties of the machine.

This Jül report describes the measuring procedure applied as well as the measuring machine. Examples of the measuring results are presented in this report for each measuring task.

We would like to warmly thank the staff of the KFA Institute of Plasma Physics and, in particular, Dr. G. Waidmann, Dipl.-Ing. B. Giesen and Dipl.-Ing. M.H. Lochter for their valuable cooperation. We are also especially obliged to Professor A.C.R. Newberry of the University of Kentucky (USA) who assisted in solving a number of mathematical problems in his capacity as a visiting scientist at the KFA's Central Institute of Applied Mathematics.

We would finally like to express our thanks to the staff members of the Central Electronics Laboratory of the KFA for their efficacious cooperation, in particular to

- *J. Hotfilter and K. Dilling who carried out the design work,*
- *N. Kress, R. Hesse, H. Müntz and C. Noteborn who manufactured the mechanical parts of the measuring apparatus and installed the measuring machine in TEXTOR,*
- *G. Breuer and U. Sieling who carried out the programming,*
- *H. Larue and H. Roeder who performed the electronic work*
- *as well as Mrs. M.L. Klein who was responsible for the extensive secretarial work involved.*

The authors are also grateful to Dipl.-Ing. K.F. Rittinghaus, head of the General Electronics Division of the ZEL, for his generous support in the execution of the work.

They furthermore wish to thank Ms. M. Heinz, head of the Translation Service at the KFA Jülich, for her meticulous translation of the Jül-Report 1816–1982 into English, as well as for corrections and proofreading involved.

Jülich, November 25, 1982

Hp. Eulenberg   B. Steffen   H. Thyssen

Abstract

This report describes a measuring apparatus controlled by the PDP-11/40 process computer and used for measuring the transient magnetic fields in the Jülich TEXTOR tokamak machine. The measuring results were moreover used for numerical off-line computation of the amplitudes and time constants of the exponentially decaying fractions of the magnetic field which are caused by eddy currents in the metal parts of the machine.

Six Hall field probes mounted on a rail-guided test van were placed by computer command in 29 measuring positions evenly distributed on the machine periphery. The time-dependent vertical and radial components of the magnetic induction were alternatively measured in the horizontal and vertical direction using a Hall field probe in three equidistant measuring points lying on the cross-section surface of the toroidal vacuum vessel of the machine.

Examples of the measuring results are presented in the last chapter of this report.

Contents

demodulating the measuring signals generated according to the ramp or half-pulse method 32

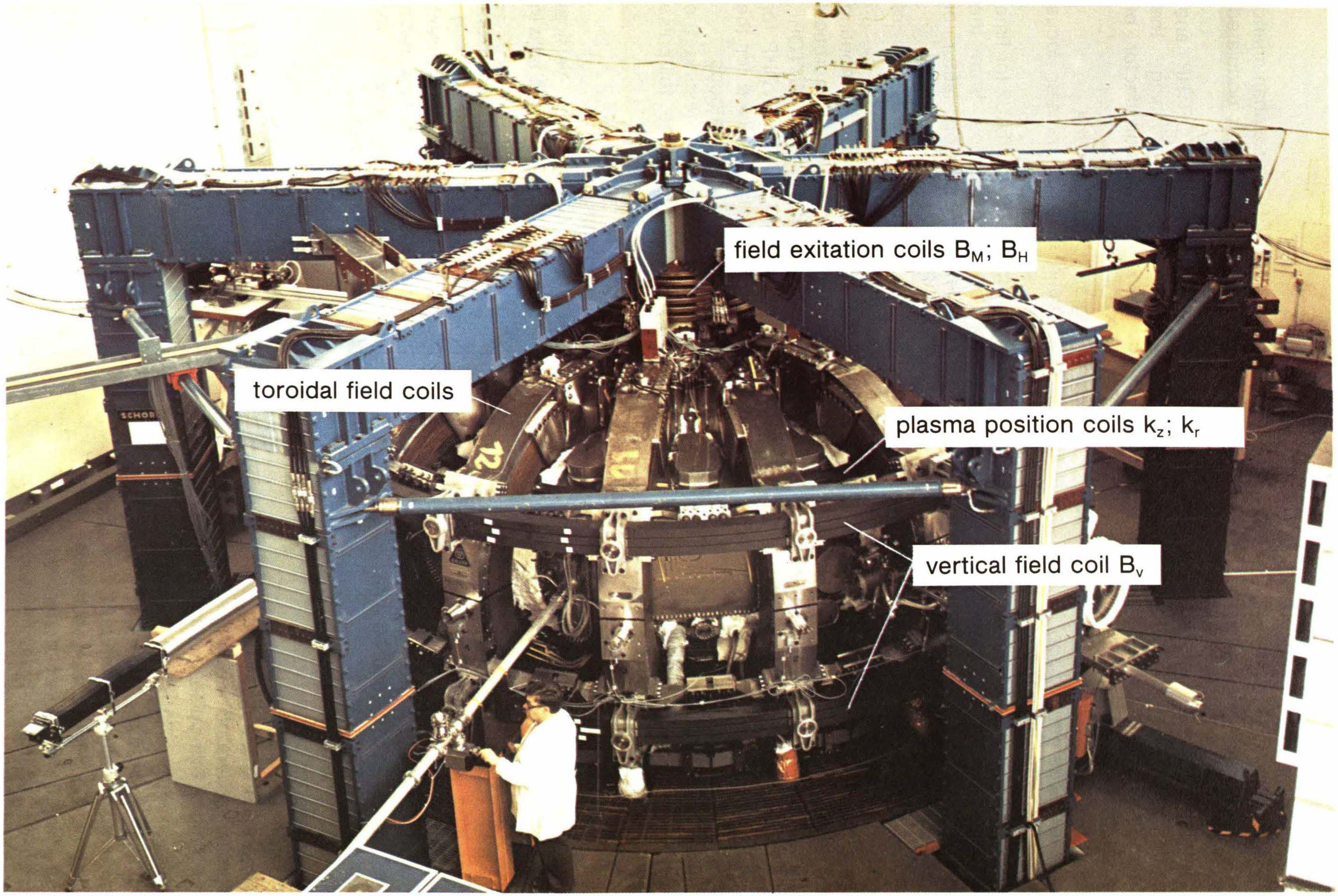

Figure 1
TEXTOR with its coil configuration

1. Introduction

The present report describes the methods and measuring devices used for measuring transient magnetic fields in the TEXTOR TOKAMAK machine and shows the measuring results obtained. It is furthermore demonstrated how the amplitudes and time constants of exponentially decaying magnetic field fractions, produced by the eddy currents flowing in the metal parts of the machine, are determined from the measured data acquired.

The time-dependent vertical and radial components of magnetic induction produced by the vertical coil, the magnetizing coil BM and the correction coils K_z and K_r were measured in three preset points on the cross section of the vacuum vessel of the machine at 29 measuring levels evenly distributed over the periphery of the machine (underneath one and between two toroidal field coils).

The time dependence of six components of magnetic induction (3 vertical, 3 radial components) as well as that of the field of the feeder cable carrying the excitation current were measured during the three-second magnetic field injection using AC-excited Hall field probes of the type SBV 585-S1*. The measured data of the measuring voltages sampled at timing invervals of 4 μs and digitized with 12 bit amplitude resolution were stored in an eight-channel transient recorder. One digital storage device with a storage capacity of 8192 measured data was allocated to each of the eight measuring channels.

The data accumulated in the storage devices of the transient recorder during a measuring cycle were taken over for further processing by the PDP-11/4o process computer during the five-minute pause.

The computer also performed the demodulation of the seven amplitude-modulated measuring voltages (6 magnetic field, 1 excitation current measuring voltage) with the aid of the time function of the AC drive current of the Hall field probes stored in the eighth channel of the transient recorder.

The measured data sequences obtained by measuring the ripple of the vertical magnetic field caused by the current converters and by measuring the time-dependent ignition field BM were displayed graphically using a plotter.

The measured data sequences obtained by measuring the time constants with which the eddy current magnetic fields decay were used to compute a complex transmission factor whose frequency dependence describes the magnetic properties of TEXTOR and from which the time constants and the amplitudes of exponentially decaying eddy current magnetic fields were computed.

The entire measuring operation was automated by means of the process computer. The computer not only ensured the evaluation of current measurements required for control purposes, but also the proper positioning of the test van built from nonconducting material and carrying the Hall field probe supports on the circular rail of synthetic resin-compressed wood in the vacuum vessel of TEXTOR (Figure 2).

* Siemens make

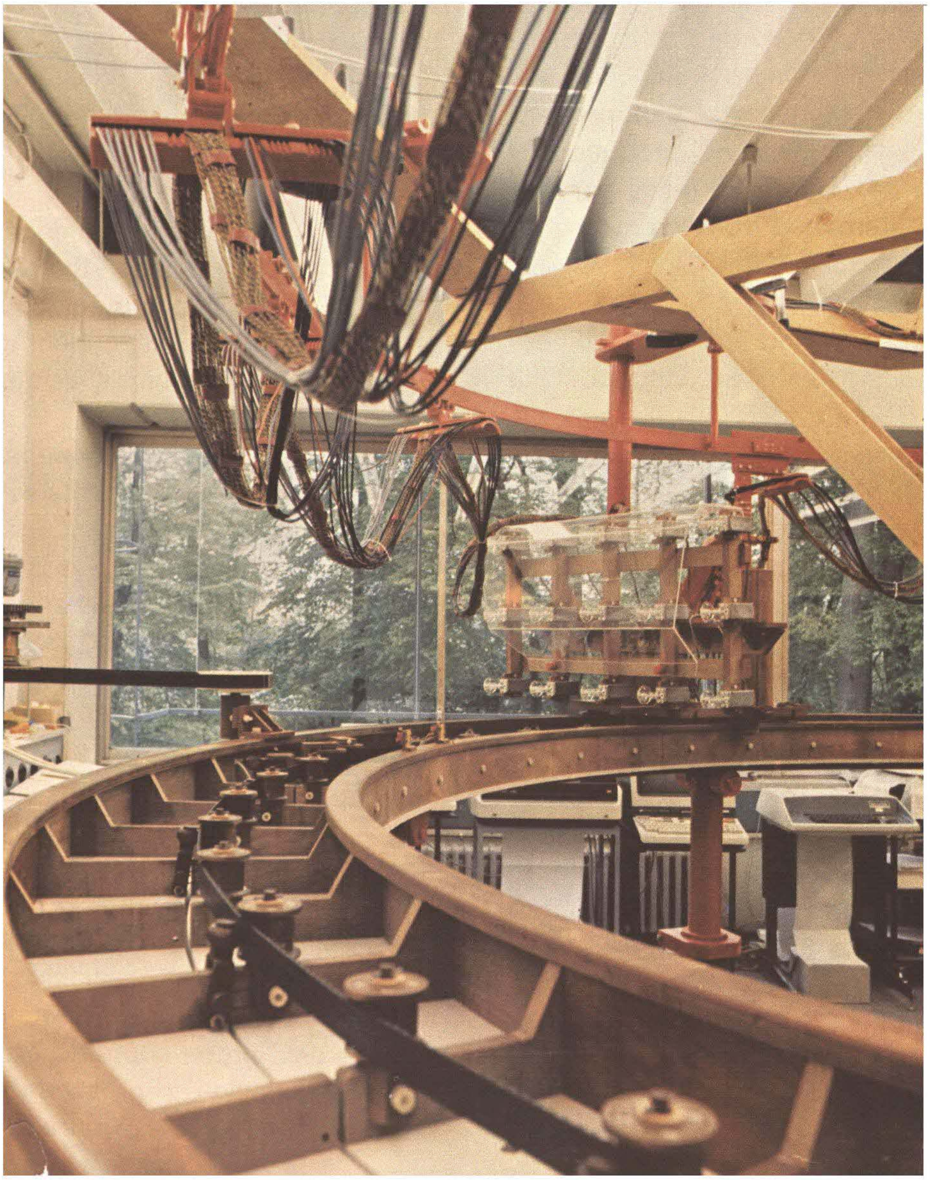

Figure 2
Experimental set-up of the rail with the test van carrying the Hall field probes

2. Measurement Techniques Applied

Hp. Eulenberg

This chapter describes the methods used for measuring the transient magnetic fields with utmost accuracy and for determining the time constants of exponentially decaying eddy current effects via transfer locus measurements.

2.1 Methods of measuring transient magnetic fields

The transient magnetic fields were measured with Hall field probes. Two field probes of a measuring point in the TEXTOR vacuum vessel, offset by 90° in the surface normal, were arranged in such a way that one of them served to measure the time-dependent radial component, and the other one for measuring the time-dependent vertical component of magnetic induction (Figure 3). Three of these dual field probes could be built optionally onto a probe holder mounted horizontally or vertically on a test van (Figure 19, Figure 20). In both cases, the probe arranged in the middle was on the mid-plane and on the mid-radius of the machine. The distance from the other two dual field probes was 47 cm in the horizontal and 20 cm in the vertical direction.

It is a well-known fact that quite a number of error voltages[1] must generally be taken into consideration when measuring with Hall field probes, which can distort the measuring result if their influence becomes too large or if they are not suppressed.

The Siemens Hall field probe SBV 585-S1 was used for measuring the transient magnetic fields of TEXTOR. The signal obtained was basically distorted by the zero residual voltage and, in particular, by the inductive error voltage, so that these had to be suppressed. Amplitude-dependent errors, such as linearity errors and measuring errors caused by the planar Hall effect, were negligibly small due to the very good linearity characteristics of the Hall field probe employed and, above all, due to the relatively low maximum field strength of about 100 mT.

The zero residual voltage is a voltage occurring at the signal terminals of a Hall field probe in the absence of induction, if the signal contacts of the probe are not exactly on a potential line of the flow field produced by the drive current flowing through the electrical system of the probe. The zero residual voltage superimposed on the measuring voltage was measured before starting the magnetic field injection and taken into consideration in the later evaluation of measurement results.

The inductive error voltage is a voltage induced by the magnetic field to be measured into the feed wires of the Hall field probe and into the wiring of the preamplifier located in the measuring field. The 40 m long lines carrying the amplified measured signal were dragged along behind the test van carrying the field probes by means of a cable transport device (Figure 2).

The inductive error voltages could be suppressed significantly, however not sufficiently (residual fraction: approx. 20 % of the measuring voltage) by twisting the feed wires of the Hall field probe and of all signal lines, by forming conductor loops as small as possible during wiring of the preamplifier and by their appropriate orientation with respect to the main direction of the transient magnetic field to be measured.

For suppressing the remaining inductive error voltage, a very effective method was developed utilizing the modulator properties of the Hall field probe.

The AC drive current of 10 kHz and 2 kHz flowing through the Hall field probe modulated the measured signal of the transient magnetic fields to be measured in the amplitude, so that the information was contained in the sidebands of the measured signal grouped around the frequency of the AC drive current.

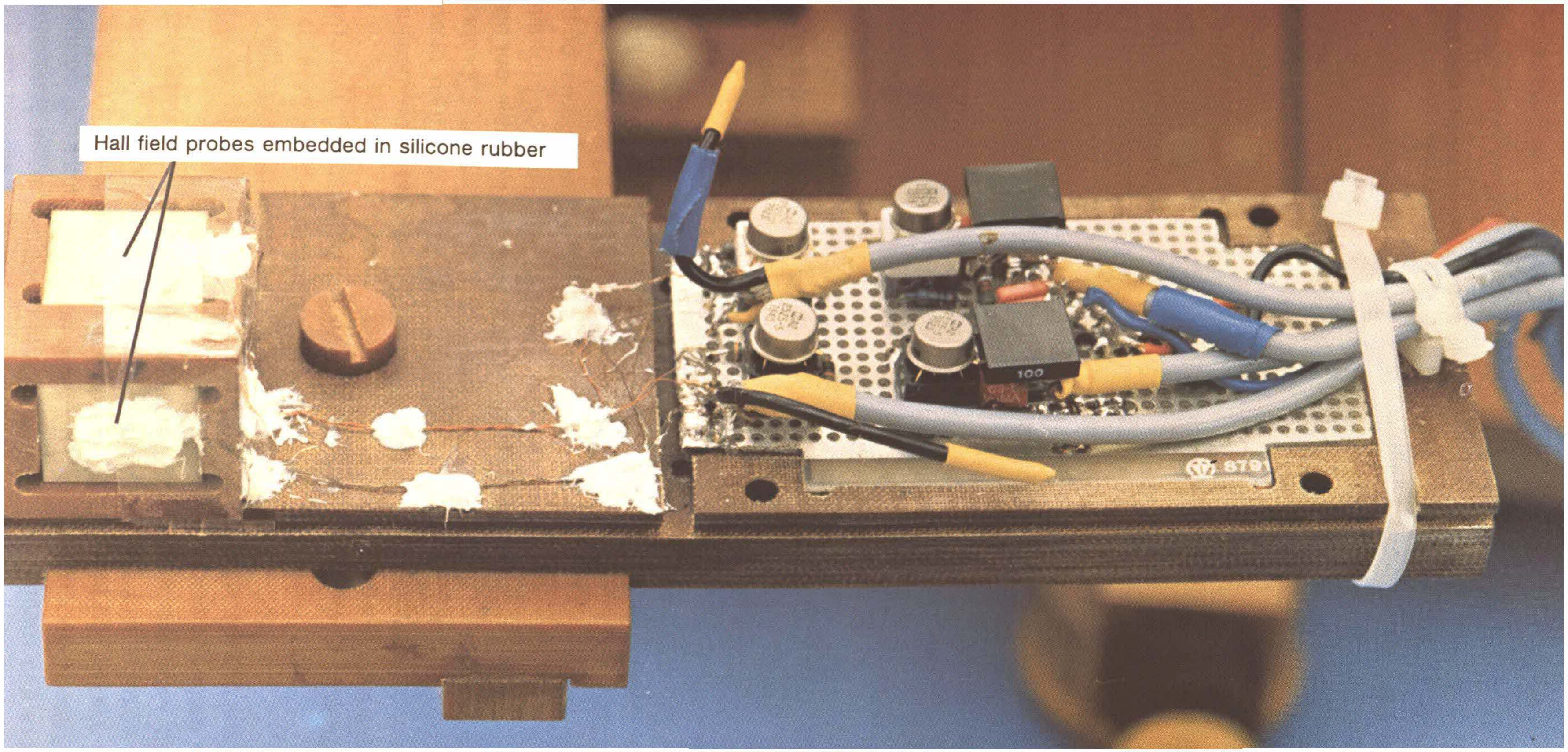

Figure 3
Hall field probe support with measuring voltage preamplifiers

In this way, it was possible to spectrally separate the measured data in the spectrum of the terminal voltage of the Hall field probe from the frequency fractions produced by the inductive zero voltage in the base band.

These disturbing frequency fractions of the spectrum of the terminal voltage of the Hall field probe could be suppressed by means of an adequately dimensioned synchronous demodulator, so that the influence of the induced error voltage on the measuring result could be eliminated. Synchronous demodulation could be carried out by a computer program since the sampled values of the measuring voltage were stored in the computer in the form of numerically given sampling sequences. The advantages as compared to demodulation with hardware demodulators was, among other things, that the extensive adjustment and symmetrizing operations otherwise required for multichannel arrangements could be omitted.

2.2 Demodulation of the measuring voltage using a process computer

The mode of operation of a synchronous demodulator of analog design and its basic configuration are shown in Figure 4. By multiplying the measuring voltage by the AC reference voltage of the drive current frequency f_T in the multiplier, as shown in Figure 4c, the spectrum of the measuring voltage (Figure 4b) was converted in such a way that all disturbing frequency fractions could be suppressed with the RC low-pass filter installed behind. The realization of the multiplier was very simple when simulating the synchronous demodulator in the computer. A single command was sufficient to carry out the multiplication of the measured value sequence of the sampled terminal voltage of the Hall field probe by the measured value sequence of the sampled sinusoidal reference voltage which was also used to generate the AC drive current flowing through the Hall field probe.

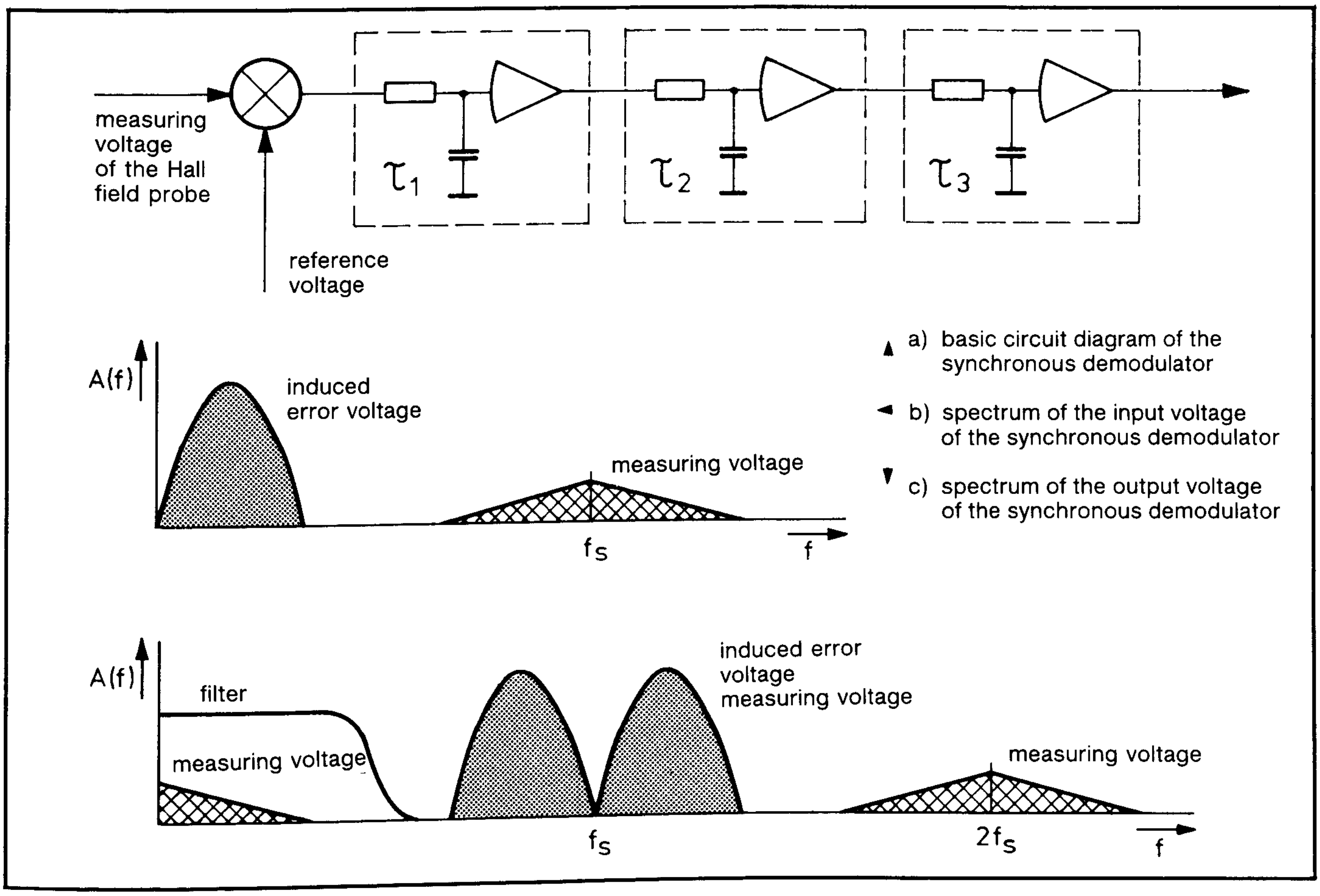

Figure 4
Design and mode of operation of a synchronous demodulator

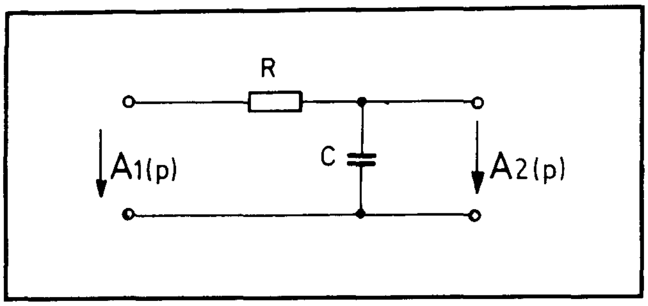

Figure 5
Simple RC low-pass filter

The three-stage low-pass filter installed behind the multiplier had been simulated as a digital filter using a process computer.

In search of the topology of the digital filter circuit and the associated run of the simulation program, the transfer function of the RC low-pass filter shown in Figure 5 and applicable to continuous signals

$$H(p) = \frac{A_2(p)}{A_1(p)} = \frac{1}{1+p\tau} \qquad \tau = R \cdot C$$

was used together with the bilinear transformation

$$p = \frac{2}{\Delta T} \cdot \frac{z-1}{z+1} \qquad \Delta T = \text{sample time}$$

to obtain the Z transform applicable to sampled functions

$$H(z) = \frac{A_2(z)}{A_1(z)} = \frac{1+z^{-1}}{(2\frac{\tau}{\Delta T}+1)-(2\frac{\tau}{\Delta T}-1)z^{-1}}$$

The factor z^{-1} implies that the value of the sampled function delayed by one clock pulse should be used for computing the actual sampling value at the filter output. The structure required for the digital filter could be read from the above equation transposed as follows:

$$A_2(z) = \frac{2\frac{\tau}{\Delta T}-1}{2\frac{\tau}{\Delta T}+1} \cdot z^{-1} \cdot A_2(z) + \frac{1}{2\frac{\tau}{\Delta T}+1} \cdot z^{-1} \cdot A_1(z) + \frac{1}{2\frac{\tau}{\Delta T}+1} \cdot A_1(z)$$

In this way, the circuit of a low-pass filter designed as a digital filter, as shown in Figure 6, and the relation of the filter coefficients C_1 and C_2 with the limiting frequency or time constant τ of the low-pass filter were found.

The program for computing the measured value sequence of the sampled output function of this filter, which executed the computer operations preset by the circuit of the digital filter, is extremely simple. As can be seen in the flow chart (Figure 7), the sample result of the output time function A(2) must be zeroed at the beginning (M = 1) of sampling the input time function A(1). This is necessary because the output voltage of a low-pass filter is zero at the moment of turn-on. For all M = M2 sample results of the input function A(1) the sample results of the output function A(2) = UA(M) of the filter are computed, and the sample result delayed by one clock pulse (z^{-1}) in the next program run is stored in the memory S1.

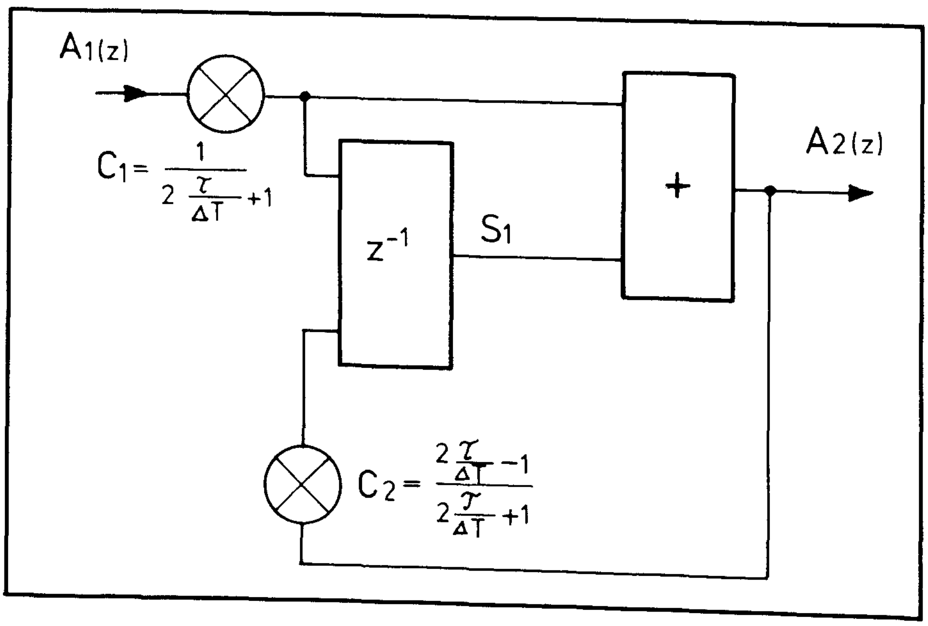

Figure 6
Circuit diagram of a digital filter low-pass

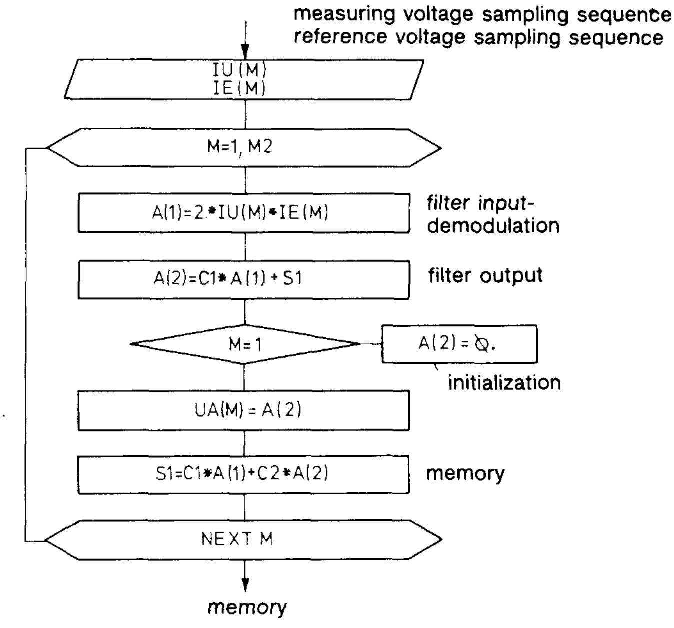

Figure 7
Flow chart for simulating the digital filter of Figure 6 in a computer

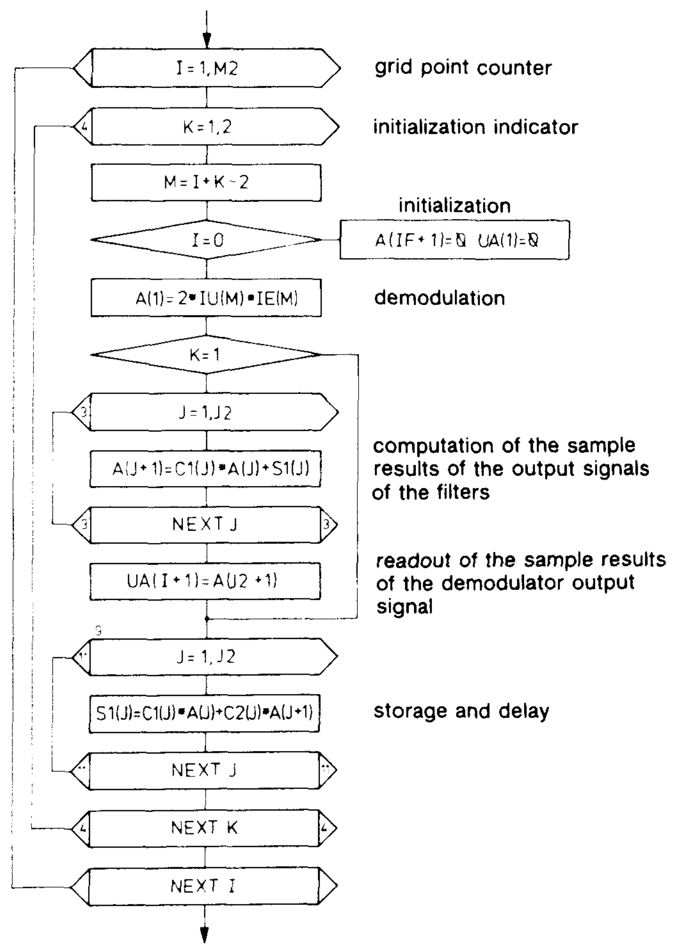

Figure 8
Software synchronous demodulator with J2 low-pass filter stages

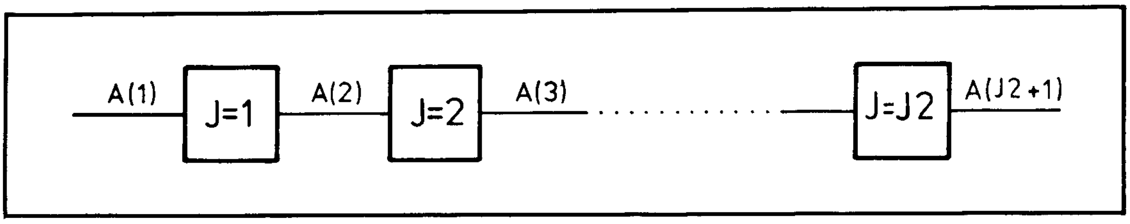

Figure 9
Iterative network of the J2 decoupled RC low-pass filters

Such a filter fulfilled its function without any problems provided that its input signal did not contain any jumps. However, since the measuring voltage could contain voltage jumps due to the induced error voltage, the starting conditions in the memory S1 had to be set anew with each voltage that occurred. It was not known, of course, when this jump occurred.

This difficulty could be overcome by generally recomputing the stored value S1 when computing the sample result of the filter output time function following next, irrespective of the occurrence of a voltage jump. As can be seen from the flow chart in Figure 8, this initialization was carried out in the memory S1(J) in the K loop with K = 1. With K = 2 the program then computed the next sample result UA(I + 1) of the filter output signal and determined the storage value S1(J) for subsequent computation of the sample value. Both S1(J) values were identical as long as no voltage jumps occurred.

The low-pass filter required for sideband suppression in the synchronous demodulator consisted of J2 decoupled RC low-pass filters whose transmission behaviours were simulated in the J loops of the program in Figure 8. A(J) represented the input, A(J + 1) the output of an RC low-pass filter (Figure 9).

2.3 Transfer locus method for determining the eddy current time constants

When processing statistically disturbed measuring signals, the disturbances are largely suppressed by integration of the measuring voltage with respect to time. For the investigation of time-dependent field fractions generated by the eddy currents flowing through the metal parts in TEXTOR, an integral transformation - the Fourier transformation - was therefore used with which the time function can be reproduced as a transform in a complex plane. The quotient of the Fourier transform of the time-dependent output variable - here of magnetic induction - and the Fourier transform of a suitably selected input variable gives a complex transmission factor depending on a variable frequency whose graphical representation is known as transfer locus. Provided that the TEXTOR machine behaves like a linear system with regard to magnetic field generation, the transfer locus completely describes its transient behaviour and, thus, the influence of the eddy current effects involved.

The equivalent circuit shown in Figure 10 is intended to illustrate, as an example, which complex transmission factor should be selected to ensure that only the eddy current effects are described and that the factor is not influenced by the internal resistance of the generator producing the excitation current $i_p(t)$.

When using the regularities of multiply coupled magnetic circuits for computing the complex transmission factor it may first of all be assumed that the magnetic field is measured in the measuring point by means of a pick-up coil whose no-

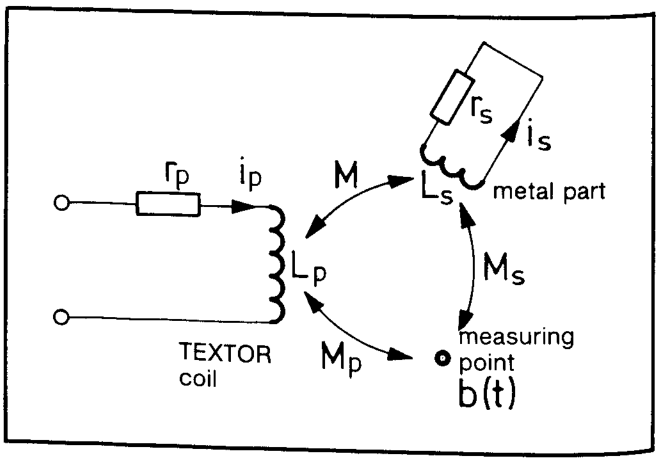

Figure 10
Equivalent circuit diagram of the magnetic circuit with an eddy current circuit

load voltage u_m must be integrated. However, a Hall field probe measures the magnetic induction

$$b(t) = \frac{1}{n\Delta A} \int u_m(t)dt$$

ΔA = winding area of the pick-up coil and active area of the Hall field probe
n = number of turns of the pick-up coil

The equations for the magnetically coupled circuits

$$0 = M \frac{di_p(t)}{dt} + r_s i_s(t) + L_s \frac{di_s(t)}{dt} \quad \text{(eddy currrent circuit)} \quad \text{eq. 2.3-1}$$

$$u_m = M_p \frac{di_p(t)}{dt} + M_s \frac{di_s(t)}{dt} \quad \text{(measuring circuit)} \quad \text{eq. 2.3-2}$$

were used for computing the time integral of the induced voltage $u_m(t)$

$$y(t) = \int u_m(t)dt$$

which is a measure of the magnetic induction in the measuring point.

Eq. 2.3-2 is used to obtain

$$y(t) = M_p i_p(t) + M_s i_s(t). \quad \text{eq. 2.3-3}$$

It is possible to measure the excitation current $i_p(t)$ but not the eddy current $i_s(t)$. However, the latter is linked with the excitation current via eq. 2.3-1. The following is obtained for the Fourier transform of u(t) using eq. 2.3-2 and eq. 2.3-3

$$F\{y(t)\} = M_p \frac{1+j\omega \frac{L_s}{r_s}\left(1-\frac{MM_s}{M_pL_s}\right)}{1+j\omega \frac{L_s}{r_s}} \cdot F\{i_p(t)\}.$$

The complex transmission factor

$$A_o(j\omega) = \frac{F\{y(t)\}}{F\{i_p(t)\}} = M_p \frac{1+j\omega \frac{L_s}{r_s}\left(1-\frac{MM_s}{M_pL_s}\right)}{1+j\omega \frac{L_s}{r_s}} \quad \text{eq. 2.3-4}$$

satisfies the condition imposed at the beginning that the internal resistance of the excitation current generator has no influence on the transmission factor. The transfer loci measured on TEXTOR are defined by eq. 2.3-4.

It is also of general interest to know what the transfer locus for an eddy current time constant looks like. Eq. 2.3-4 shows the ratio L_s/r_s to be a time constant of the eddy current circuit. The quotient $(M \cdot M_s)/(M_p \cdot L_s)$ contains information about the position of the measuring point with respect to the field excitation coil (M_p) and the eddy current circuit (M_s). M/L_s is a quantity fixed by the design of the machine.

$$x = \frac{MM_s}{M_pL_s}, \quad \text{eq. 2.3-5}$$

the position-dependent parameter x, can assume values between zero and one.

$$0 < x < 1 \quad \text{eq. 2.3-6}$$

If there is no field disturbance by the eddy current, then $M_s = 0$, i.e.

$$x = 0$$

applies in the absence of eddy current influence.

In this case, the transfer locus is degenerated into a point because of

$$A_o(j\omega) = M_p$$

which lies on the real axis of the complex plane and is determined by M_p, that is by the distance of the measuring point from the field excitation coil.

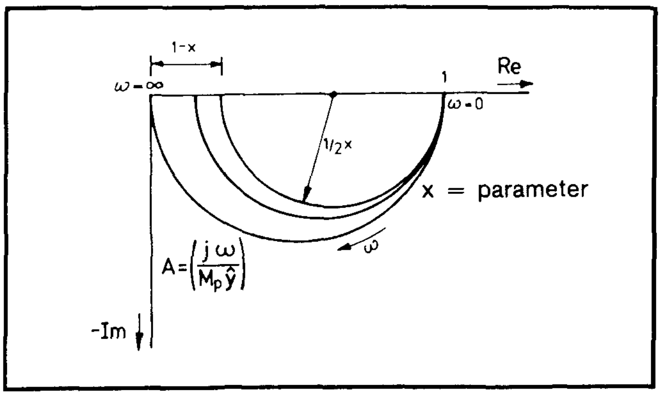

Figure 11
Normalized transfer locus for an eddy current circuit

The points of the transfer locus $A_o(j\omega)$ measured on TEXTOR were normalized in such a way that the locus point lying on the real axis at the circuit frequency $\omega = 0$ always assumed the value 1.

The complex transmission factor for an eddy current circuit (eq. 2.3-4) normalized to this effect,

$$A(j\omega) = \frac{1+j\omega\tau_s(1-x)}{1+j\omega\tau_s} \qquad \tau_s = \frac{L_s}{r_s} \quad \text{eddy current time constant}$$

whose transfer locus can be seen in Figure 11, shows the magnetic field system of TEXTOR to be a minimum-phase system with low-pass filtering behaviour.

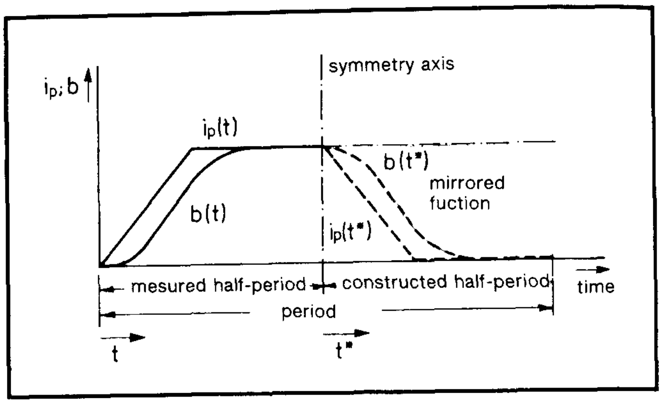

Figure 12
Method of complementing the measured section of the excitation current and field function to form a periodic signal according to the half-pulse principle

2.3.1 Fundamentals for experimentally determining the Fourier integrals

Transmission factors are usually measured by means of AC voltage generators with adjustable frequency. This method could not be used for measuring the complex transmission factor for cost reasons because of the field excitation currents lying in the kA range.

In order to avoid additional investments, the transmission factors had to be measured using the current converters envisaged for the operation of TEXTOR. They generate field excitation currents containing harmonics which were used for measuring the frequency-dependent complex transmission factor. The latter was computed by quotient formation from the complex Fourier transform of the measuring signal which is proportional to the magnetic induction and from the transform of the signal which is proportional to the field excitation current.

The existence of periodic time functions was assumed for the Fourier analysis required for determining the amplitudes and phases of the harmonics. However, this assumption only proved to be true initially for field measurements in the correction coils K_z and K_r. In addition to a steady field, the field excitation current of these coils produced a periodic magnetic field obliterated exponentially in time during the three seconds of field injection with a repetition frequency of approx. 25 Hz. The computer programs with which the Fourier transformation of these time-dependent fields was carried out are characterized as '... **according to the full-pulse principle (VP)**'.

The periodicity of the signal to be analyzed, which is necessary for the Fourier analysis, is not provided for examining the eddy current effects effective upon turn-on of the three-second vertical field. In order to be able to use this analytical technique despite this deficiency, two methods were developed for constructing a periodic signal from the dependence of the magnetic field on time occurring during turn-on of the field excitation current, exploiting the symmetry properties of periodic output signals of linear time-invariant systems.

With the so-called '**half-pulse technique (HP)**', measurements using the transient recorder had to be extended beyond the pulse top after turning on the linearly rising field excitation current until the magnetic fields produced by the eddy currents had decayed to about 10^{-4}.

If $i_p(t)$ describes the excitation current and b(t) the time-dependent magnetic field recorded during the measuring time T_m, it will be possible to compute the function values $i_p(t)$ and $b(t^*)$ according to

$$i_p(t^*) = \hat{i}_p - i_p(t) \qquad \text{eq. 2.3.1-1}$$

and

$$b(t^*) = \hat{b} - b(t) \qquad \text{eq. 2.3.1-2}$$

$0 < t < T_m$ (measuring cycle)
$0 < t^* < T_m$ (mirroring)

which are necessary for complementing the functions to obtain a full period of an imaginary periodic function. This was based on the assumption that the excitation current is lowered to zero with the same time dependence as during its increase upon turn-on. The even-numbered harmonics are not present in the Fourier spectrum of these functions because of the pulse duty factor of two selected in this way.

The **ramp technique (RA)** permitted a periodic signal to be composed with a pulse duty factor of two from the field pattern produced by an excitation current ramp. The fraction growing exponentially with time - dashed fraction in the 1st quadrant of Figure 13 - was determined from the field pattern b(t) measured in quadrant 1

$$\ell(t) = \left.\frac{db(t)}{dt}\right|_{t=\frac{T_w}{4}} \cdot t - b(t). \qquad \text{eq. 2.3.1-3}$$

This function was used to compute the field pattern in the 2nd quadrant at constant excitation current

$$b(t) = b(t=\frac{T_w}{4}) + \ell(t-\frac{T_w}{4}), \qquad \frac{T_w}{4} < t < \frac{T_w}{2} \qquad \text{eq. 2.3.1-4}$$

The following applied to the 3rd quadrant with time-proportional reduction of the excitation current:

$$b(t) = \left[b(t=\frac{T_w}{4}) + \ell(t=\frac{T_w}{4})\right] - b(t-3\frac{T_w}{4}). \qquad \text{eq. 2.3.1-5}$$

$$\frac{T_w}{2} < t < 3\frac{T_w}{4}$$

The field pattern in the 4th quadrant was determined from

$$b(t) = b(t=3\frac{T_w}{4}) - \ell(t-3\frac{T_w}{4}) \qquad \text{eq. 2.3.1-6}$$

$$3\frac{T_w}{4} < t < T_w$$

because of the absence of the field excitation current i_p.

Now that the conditions for a Fourier harmonics analysis were established, the task was to ascertain the relationship between the coefficients of the Fourier series and constants of the Fourier transform and the manner in which the complex transmission factor can be determined from measured data.

The Fourier transform of a time function f(t), for which f(t) = 0 with t<0, is generally defined by

$$F(j\omega) = \int_0^\infty f(t)\,\ell^{-j\omega t}\,dt.$$

The following results when described in the real and imaginary part

$$F(j\omega) = \int_0^\infty f(t)\cos\omega t\,dt - j\int_0^\infty f(t)\sin\omega t\,dt.$$

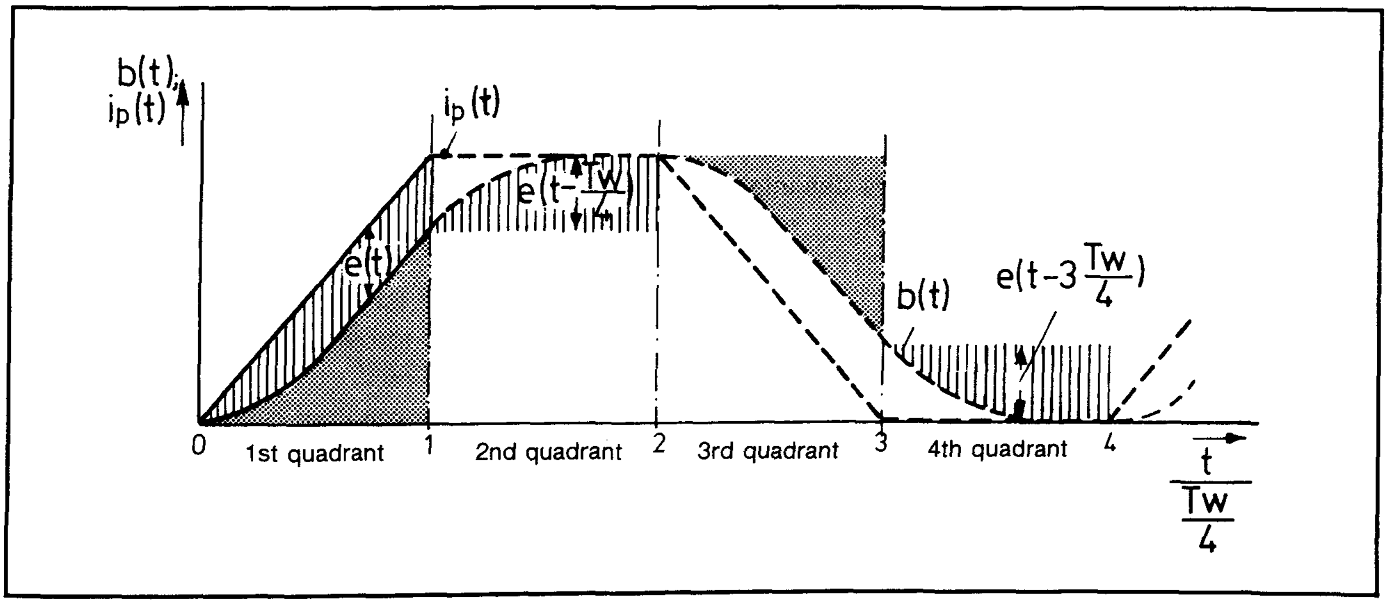

Figure 13
Method of complementing the field pattern produced by an excitation current ramp to form a periodic function according to the ramp principle

$F(j\omega)$ applies to all frequencies, i.e. also for the excellent discrete frequencies

$$\omega_n = n \cdot \frac{2\pi}{T_w} \qquad n = \{1;\ 2;\ 3 \ldots\} \quad T = \text{period}$$

of the discrete Fourier spectrum, so that the following applies to the frequencies ω_n:

$$F(j\omega_n) = \int_0^\infty f(t)\cos(n\,\frac{2\pi}{T_w}\cdot t)\,dt - j\int_0^\infty f(t)\sin(n\,\frac{2\pi}{T_w}\cdot t)\,dt.$$

Discrete points of the transfer locus $A(j\omega)$ could accordingly be determined with respect to

$$A(j\omega)\Big|_{\omega=n\frac{2\pi}{T}} = \frac{\operatorname{Re} F\{b(t)\}\Big|_{\omega=n\frac{2\pi}{T_w}} - j \operatorname{Im} F\{b(t)\}\Big|_{\omega=n\frac{2\pi}{T_w}}}{\operatorname{Re} F\{i_p(t)\}\Big|_{\omega=n\frac{2\pi}{T_w}} - j \operatorname{Im} F\{i_p(t)\}\Big|_{\omega=n\frac{2\pi}{T_w}}}.$$

eq. 2.3.1-7

It remains to be checked under which conditions the real and imaginary parts of eq. 2.3.1-7 can be determined with a harmonics analysis of the field and excitation current function.

Except for the factor $2/T_w$, these integrals are identical with the integrals

$$S_n = \frac{2}{T_w}\int_0^{T_w} f(\xi)\sin(n\,\frac{2\pi}{T_w}\cdot\xi)\,d\xi$$

and

$$C_n = \frac{2}{T_w}\int_0^\infty f(\xi)\cos(n\,\frac{2\pi}{T_w}\cdot\xi)\,d\xi$$

for determining the coefficients of the Fourier series

$$f(t) = \sum_{\nu}^{\infty} S_\nu \sin(\nu\,\frac{2\pi}{T_w}\cdot t) + \sum_{\nu=0}^{\infty} C_\nu \cos(\nu\,\frac{2\pi}{T_w}\cdot t)$$

when all transient processes of the system have decayed and the integration over the time range therefore coincides with that up to infinity. In order to keep the error produced by premature truncation of the integration below $3\cdot 10^{-4}$ – resolution of the analog-digital converter – the integration of the measuring function was extended over a time approximately corresponding to the eightfold time constant with which the slowest magnetic field fractions caused by the eddy current effect decay exponentially. The imaginary part of the complex Fourier transform of $b(t)$ and $i_p(t)$ corresponds to the negative values of the sine coefficients of the Fourier series under the conditions assumed.

For a numerical computation of the points applicable to the frequencies

$$\omega = n \cdot \frac{2\pi}{T_w}$$

of the transfer locus defined by eq. 2.3.1-7, a Fourier analysis of the time function $b(t)$ and $i_p(t)$ had to be carried out, with the cosine coefficients C_n representing the real part and the negative coefficients of the sine coefficients S_n the imaginary part of the complex Fourier transform.

The numerical integration required for computing the Fourier integral was carried out according to the Simpson integration technique. This method provided most accurate results for integration of the measured values featuring statistical errors. This was found by investigations incorporating the errors of the measuring equipment, in which the integration was carried out according to the Romberg method containing as a special case the trapezoidal and integration technique as well as the integration method according to Simpson.

2.3.2 Influence of demodulation errors and of induced error voltage on the transfer locus

Since both the magnetic induction $b(t)$ and the excitation current $i_p(t)$ were measured over the magnetic field of the feeder cables of the coils using the same type of Hall field probe measuring equipment, the frequency response of the measuring equipment has no influence in a first approximation on the measuring result due to the quotient formation of the Fourier transform when computing the complex transmission factor $A(j\omega)$. It must therefore be checked whether the induced error voltage can also be suppressed in transfer locus measurements using the modulation technique.

Both the measured signal for the magnetic induction b(t) and that of the excitation current $i_p(t)$ have the time dependence

$$s(t) = \underbrace{b^*(t)\sin \omega_T t}_{\text{measured signal}} + \underbrace{A_o \frac{db^*(t)}{dt}}_{\text{inductive error voltage}} .$$

eq. 2.3.2-1

for Hall field probes operated with alternating drive current of the frequency f_T and in connection with simultaneously superimposed induced error voltage. The multiplier of the synchronous demodulator multiplies this signal by the so-called reference voltage which is sinusoidal and phase-locked towards the drive current of the Hall field probes.

$$m(t) = 2 \cdot s(t) \cdot \sin \omega_T t$$ eq. 2.3.2-2

will then be the output signal of the multiplier. The voltage $m_B(t)$ is on the multiplier output when measuring the magnetic field and the voltage $m_{ip}(t)$ when measuring the excitation current. For determining the complex transmission factor, the quotient of the Fourier transform of both voltages

$$A_m(j\omega) = \frac{F\{m_B(t)\}}{F\{m_{ip}(t)\}}$$ eq. 2.3.2-3

had to be formed. The transmission factor $A(j\omega)$ measured in this way should differ as little as possible from the transmission factor to be measured

$$A(j\omega) = \frac{F\{b(t)\}}{F\{i_p(t)\}}$$ eq. 2.3.2-4

describing the magnetic transmission properties of TEXTOR. If the influence of measuring errors is described by a complex error function $F(j\omega)$ of the type

$$A_m(j\omega) = A(j\omega) \cdot F(j\omega)$$ eq. 2.3.2-5

measurements involving a minimum of errors should be based on the condition that

$$F(j\omega) \approx 1 \qquad o < \omega < \infty$$

is satisfied. The properties of this error function will now be studied with the aid of the Laplace transform using the complex variable

$$p = \sigma + j\omega .$$

It is known that for $\sigma = 0$ the points of the Laplace transform are on the imaginary axis of the Laplace plane on which the searched complex transmission factor is then reproduced. Consequently, eq. 2.3.2-5 can be computed using the Laplace transform from

$$A_m(p)\Big|_{p=j\omega} = A(p)\Big|_{p=j\omega} \cdot F(p)\Big|_{p=j\omega}.$$ eq. 2.3.2-6

For the Laplace transform of the multiplier output signal, the following is obtained using eq. 2.3.2-2

$$L\{m(t)\} = M(p) = 2 \cdot L\{s(t) \cdot \sin \omega_T t\}$$
$$= \frac{1}{j}\left[S_{(p-j\omega_T)} - S_{(p+j\omega_T)}\right] ,$$

with

eq. 2.3.2-7

$$S(p) = L\{s(t)\} = \frac{1}{j}\left[B_{(p-j\omega_T)} - B_{(p+j\omega_T)}\right] + pA_o B_{(p)}$$

being the Laplace transform of the multiplier input signal s(t) (eq. 2.3.2-1). With the aid of this transform and the relation eq. 2.3.2-7 the Laplace transform of the amplitude-demodulated output signal of the multiplier is obtained

$$M(p) = B(p)$$ measuring variable

$$- \frac{1}{2}\left[B_{(p-j2\omega_T)} + B_{(p+j2\omega_T)}\right]$$ sidebands of the demodulator

$$+ p\frac{A_o}{j}\left[B_{(p-j\omega_T)} - B_{(p+j\omega_T)}\right].$$ sidebands of the inductive error voltage

eq. 2.3.2-8

It may be seen that in this relation, in addition to the transform of the measured signal B(p), the spectrally separated fractions of the undesired upper sidebands caused by demodulation and the sidebands produced by inductive error voltage occur. The sidebands produced by the demodulator are grouped around the double frequency $2f_T$ of the drive current of the Hall field probe, while the sidebands around f_T are caused by the inductive error voltage.

By means of the relation derived from eq. 2.3.2-8 for the transform to be measured

$$A_m(p) = \underbrace{\frac{B_B(p)}{B_{IP}(p)}}_{A(p)} \cdot \underbrace{\frac{1-\frac{1}{2}\cdot\frac{B_B(p-j2\omega_T)}{B_B(p)}+\frac{B_B(p+j2\omega_T)}{B_B(p)} + p\,\frac{A_B}{j}\,\frac{B_B(p-j\omega_T)}{B_B(p)}-\frac{B_B(p+j\omega_T)}{B_B(p)}}{1-\frac{1}{2}\,\frac{B_{IP}(p-j2\omega_T)}{B_{IP}(p)}+\frac{B_{IP}(p+j2\omega_T)}{B_{IP}(p)} + p\,\frac{A_{IP}}{j}\,\frac{B_{IP}(p-j\omega_T)}{B_{IP}(p)}-\frac{B_{IP}(p+j\omega_T)}{B_{IP}(p)}}}_{F(p)}$$

eq. 2.3.2-9

the error function F(p) is obtained which indicates the influence exerted by the sidebands produced by demodulation and by inductive error voltage on the transmission factor $A(p)_{p=j\omega}$ of TEXTOR to be measured and, above all, whether and under which conditions the inductive error voltage can be adequately suppressed by means of the modulation technique used for magnetic field measurements.

The denominator of the complex error function features the ratios B_{Ip} $(p \pm j\omega_T)$ to $B_{Ip}(p)$ and $B_{Ip}(p \pm j2\omega_T)$ to $B_{Ip}(p)$. The magnitude of these ratios is solely determined by the spectral properties of the field excitation current $i_p(t)$. A converging signal spectrum is the necessary condition satisfied in this case that the spectral amplitudes are substantially smaller at the frequencies $\omega \pm \omega_T$ and $\omega \pm 2\omega_T$ than those at the signal frequency ω, so that

$$B_{I_p}(p \pm jn\omega_T)\Big|_{p=j\omega} \ll B_{I_p}(p)\Big|_{p=j\omega}, \quad n = \{1;2\}$$

eq. 2.3.2-10

Consequently, the frequency of the drive current f_T flowing through the Hall field probe should be as high as possible in comparison with the frequency of the excitation current i_p, for this is the condition under which the denominator of the complex error function approaches the value 1 on the real axis of the number plane and the value 0 on the imaginary axis.

Besides the signal properties, also the transmission properties of the object to be measured enter into the ratios of the Fourier transform of the numerator of the error function. The Fourier transform of the time-dependent induction b(t) is linked according to eq. 2.3.2-4 with the Fourier transform of the excitation current via the complex transmission factor $A(j\omega)$ by

$$B_B(p)\Big|_{p=j\omega} = A(p)\Big|_{p=j\omega} \cdot B_{I_p}(p)\Big|_{p=j\omega}.$$

eq. 2.3.2-11

The Fourier transforms of the sidebands of the amplitude-modulated measuring voltage are obtained by shifting the frequency scale to:

$$B_{B(p \pm jn\omega_T)}\Big|_{p=j\omega} = A_{(p \pm jn\omega_T)}\Big|_{p=j\omega} \cdot B_{I_p}(p \pm jn\omega_T)\Big|_{p=j\omega}.$$

$$n = \{1;2\}$$

eq. 2.3.2-12

As was shown by the example in chapter 2.3, A(p) takes the course of a minimum-phased low-pass filter. In the example discussed in this chapter, the transmission factors

$$A_{(p \pm jn\omega_T)}\Big|_{p=j} \qquad n = \{1;2\}$$

eq. 2.3.2-13

decisive for the sidebands converge with sufficiently large ω_T toward the value (1-x) which depends on the measuring position. Since the condition established by eq. 2.3.2-10 also applies to the numerator of the error function, the numerator's value also tends towards the value 1 with sufficiently large ω_T.

It is thus demonstrated that the complex transmission factor $A(j\omega)$ of TEXTOR can be determined by measurement techniques via quotient formation of the Fourier transform of the amplitude-modulated magnetic field measuring voltage superimposed by induced error voltage with the Fourier transform of the excitation current.

The selection of a sufficiently high frequency of the AC drive current flowing through the Hall field probe is a prerequisite for optimal suppression of the sidebands produced by demodulation and of the error voltages coupled into the feedlines of the Hall field probe by induction.

In order to make quantitative statements on the size of the measuring error, the error was computed for a time-proportional excitation current increase in a magnetic field system with 1 time constant with the eq. 2.3.2-14 derived from eq. 2.3.2-9 with due regard to eq. 2.3.2-13.

$$F(p) = \frac{1-Z_1(p=j\omega) + p\cdot Z_2(p=j\omega)}{1-N_1(p=j\omega) + p\cdot N_2(p=j\omega)}$$

$$Z_1(p=j\omega) = \frac{1}{2}\left[\frac{A(p-j2\omega_T)}{A(p)}\cdot\frac{B_{IP}(p-j2\omega_T)}{B_{IP}(p)} + \frac{A(p+j2\omega_T)}{A(p)}\cdot\frac{B_{IP}(p+j2\omega_T)}{B_{IP}(p)}\right]_{p=j\omega}$$

$$Z_2(p=j\omega) = \frac{A_B}{j}\left[\frac{A(p-j\omega_T)}{A(p)}\cdot\frac{B_{IP}(p+j\omega_T)}{B_{IP}(p)} - \frac{A(p+j\omega_T)}{A(p)}\cdot\frac{B_{IP}(p+j\omega_T)}{B_{IP}(p)}\right]_{p=j\omega}$$

$$N_1(p=j\omega) = \frac{1}{2}\left[\frac{B_{IP}(p-j2\omega_T)}{B_{IP}(p)} + \frac{B_{IP}(p+j2\omega_T)}{B_{IP}(p)}\right]_{p=j\omega}$$

$$N_2(p=j\omega) = \frac{A_{IP}}{j}\left[\frac{B_{IP}(p-j\omega_T)}{B_{IP}(p)} - \frac{B_{IP}(p+j\omega_T)}{B_{IP}(p)}\right]_{p=j\omega} \quad \text{eq. 2.3.2-14}$$

```
RUN FEHLMO
PROGRAM*FEHLMO.FTN
PROJECT TEXTOR
ERRORS IN TRANSFER LOCUS DETERMINATION DUE TO DEMODULATION

POSITION FACTOR (0<X<1.0000) X = 1.
TIME CONSTANT [MSEC] TAU = 8.
CARRIER FREQUENCY [KHZ] = 5.
ZERO COMPONENT - FIELD [CM**2] = 20.
ZERO COMPONENT - CURRENT [CM**2] = 0.
FIELD PROBE SENSITIVITY [MV/T] = 50.

  N      FRE ABS     FIM ABS       ARE     AIM        VRE     VIM
  1     0.00E+00    0.00E+00    1.0000  0.0000     1.0000  0.0000
  2    -0.12E-06    0.19E-09    0.9759 -0.1533     0.9759 -0.1533
  3    -0.48E-06    0.73E-09    0.9102 -0.2859     0.9102 -0.2859
  4    -0.83E-06    0.15E-08    0.8183 -0.3856     0.8183 -0.3856
  5    -0.14E-05    0.23E-08    0.7170 -0.4505     0.7170 -0.4505
  6    -0.20E-05    0.29E-08    0.6185 -0.4858     0.6185 -0.4858
  7    -0.25E-05    0.30E-08    0.5296 -0.4991     0.5296 -0.4991
  8    -0.30E-05    0.22E-08    0.4527 -0.4978     0.4527 -0.4978
  9    -0.31E-05   -0.41E-11    0.3877 -0.4872     0.3877 -0.4872
 10    -0.30E-05   -0.42E-08    0.3335 -0.4715     0.3335 -0.4715
 11    -0.21E-05   -0.11E-07    0.2884 -0.4530     0.2884 -0.4530
 12    -0.83E-06   -0.21E-07    0.2509 -0.4335     0.2509 -0.4335
 13     0.17E-05   -0.35E-07    0.2196 -0.4140     0.2196 -0.4140
 14     0.54E-05   -0.53E-07    0.1934 -0.3950     0.1934 -0.3950
 15     0.10E-04   -0.77E-07    0.1713 -0.3768     0.1713 -0.3768
TTO  --  STOP
>
```

Table 1

Program for computing the errors in transfer locus determination caused by amplitude modulation of the measuring signal

The computational results shown in Table 1 applied to a ramp rise time of the excitation current of T = 80 msec, to an eddy current time constant τ = 8 msec and to an inductive zero component in the field measuring channel of A_o = 20 cm^2*. The position factor x = 1 indicates that the point where the magnetic field is measured lies in the immediate vicinity of a TEXTOR metal part carrying eddy current. The Hall field probe has a sensitivity of 50 mV/Tesla, the frequency of the drive current being f_T = 5 kHz.

The exact values of the real part ARE and the imaginary part AIM for N = 1 to 15 transfer locus points are printed out in the two central columns of Table 1. The two columns on the right represent the real and imaginary parts VRE, VIM of the complex transmission factor determined according to the measurement technique described. A comparison of the two columns shows that both the real and the imaginary part of the two columns are identical up to the fourth place. FRE ABS and FIM ABS only show a deviation of $+10^{-5}$ in the real part and -7.7×10^{-8} in the imaginary part at the 15th transfer locus point.

The computational results obtained demonstrate the high efficiency of the described method for suppressing the very high induced error voltage (A_o* = 20 cm^2).

* A_o = inductive zero component = effective area producing the inductive error voltage

2.4 Computational determination of the time constants of eddy current effects from the measured values of a transfer locus

B. Steffen

As was shown in the preceding paragraph, a transfer locus can be computed from the data of a coil configuration. Configurations which are more complicated than the one described above will lead to more complicated analytical representations of the transfer locus, e.g. higher-degree rational functions for systems with more than one eddy current circuit. Conversely, the data of the configuration can be determined from the representation of the transfer locus. Individual points of the transfer locus can be determined by measurement. The task of mathematical processing consists in computing the analytical representation of the transfer locus from the values measured and in deriving from this representation the characteristics required, such as the time constants of the eddy current circuits formed by the TEXTOR vessel. These cannot be measured directly.

The TEXTOR vessel is too complex in its geometry to permit a restriction to a single eddy current circuit for its description. There only existed vague indications as to the least complexity required prior to beginning the measurement series. These suggested that - depending on the position of the measuring point - one to three current circuits would be sufficient for describing the magnetic properties. This results in a third-degree rational function for describing the transfer locus. Initial test computations also revealed that the result would be greatly distorted by measuring errors if higher degree approximations were attempted. The mathematical tasks are therefore as follows (P1):

The following are given:

a) a vector of measuring points x,

$$x_k = (2 \cdot k - 1) \cdot i \cdot w_o, \quad k = 1, \ldots, n, \qquad \text{eq. 2.4-1}$$

b) a complex vector of the length n of measured values f_1,

c) an error bound ε.

Required is a real parameter vector $\hat{a}$ of the length $m \leq 3$, so that for

$$r(\hat{a},x) = \frac{1 + \hat{a}_{m+1} x + \ldots + \hat{a}_{2m} x^m}{1 + \hat{a}_1 x + \ldots + \hat{a}_m x^m} \quad \text{eq. 2.4-2}$$

the following is true

$$\left| r(\hat{a},x_k) - f_k \right| < \varepsilon. \qquad k = 1,\ldots,n$$

eq. 2.4-3

The measured values f_i are known to lie approximately on a semicircle of the shape

$$|z-M| = 1-M \text{ with } 1/2 < M < 1.$$

Consequently, the numerator of $r(\hat{a},x)$ has for the most part smaller coefficients than the denominator.

For actual computation purposes, it is appropriate to replace the condition P1 by (P2):

Required is a parameter vector a', so that r(a',x) approaches the measured values f in the sense of the least squares method,

$$\sum_{k=1}^{n} (r(a',x_k) - f_k)^2 \leq \sum_{k=1}^{n} (r(a,x_k) - f_k)^2 \qquad a \varepsilon R^{2m}$$

eq. 2.4-4

and to verify in retrospect whether a' also satisfies P1. P2 gives a normal nonlinear least squares problem. There is some standard software available for its solution which, however, could not be used for reasons described further below.

Since the TEXTOR construction program required speedy measurement and evaluation operations, the evaluation software had to be established prior to the beginning of measurements. In order to ensure realistic tests despite this requirement, series of test data were provided by the ZEL (Central Electronics Laboratory) where one data set was computed in each case from known coil properties and a second determined by measurements on these coils. The measurements were optionally carried out according to the full-pulse, half-pulse or ramp technique. In this way, it was also possible to check the sensitivity of the transfer locus coefficients to measuring errors.

This procedure revealed that the unavoidable measuring errors of about 5×10^{-4} at $m = 3$ lead to an uncertainty of about 2×10^{-2} in the coefficients, depending on the position of the values measured, and that for $m = 4$ even the first place after the decimal point was not secured for these coefficients. The influence of errors could even be substantially higher for particularly unfavourable series of measurements which, however, are not to be expected in real measurements.

P2 leads to a global nonlinear minimization problem. There is at present no practicable solution approach to this problem, but there does exist a solution for the associated local problem (P3):

Required is a vector a', so that the approximation of r(a',x) to f cannot be improved by minor changes in a'.

Unfortunately, there are generally several and in unfavourable cases even an infinity of solutions to this problem which do not all satisfy also the condition P1. By careful selection of the starting point for search of the minimum and by limiting the search steps it must now be ensured that the solution of P3 found by the method selected will also solve P1. This could not be achieved satisfactorily using the software methods available, so that specific programs had to be developed. This was done in two different ways.

The first program solves P3 iteratively with respect to $m = 1, 2, 3$ until eq. 2.4-3 is fulfilled. The starting value for the case $m = 1$ is the solution of the interpolation problem which results when considering only the measured value with the smallest imaginary part which is located in the transfer locus pattern at an elevation angle of about 90°. This point constitutes a good compromise with regard to accuracy. On the one hand, it is well determined by measurements, which are increasingly difficult and less accurate with rising frequency, and, on the other hand, it is sufficiently far away from 1 in order to permit an exact interpolation.

The solution of m = 1 is taken as the starting value for m = 2, and that of m = 2 for m = 3.

The iteration is carried out in each stage as a strongly damped Newton iteration in which, unlike customary practice, the damping factor is not selected so as to achieve a maximum step length; it is rather selected firmly as a function of the goodness of fit attained so as to be very small at the beginning and to become 1 not before a very good fit is reached. This eliminated a convergence towards solutions of eq. 2.4-5, which do not solve eq. 2.4-4, execpt for one case.

In this case, the measuring errors were particularly large, on the one hand, and f_1 was by more than a quarter circle away from 1 along the transfer locus, so that even the initial approximation posed problems.

This revealed a general problem of rational approximation: The multiplication of numerator and denominator with 'almost equal' linear factors considerably changes the coefficients, but not the function values in the places considered.

The second program makes use of the fact that the coefficients of the numerator of r are substantially smaller than those of the denominator. The program therefore interchanges the numerator and denominator in eq. 2.4-2 and approximates the values 1/F by a rational function.

This procedure has the advantage that the nonlinearity of the problem caused by the denominator becomes far less apparent; on the other hand, particularly critical measured values belonging to large indices now assume greater importance. Consequently, the method failed in one case involving large measuring errors and measured values near 0. The further procedure in the second program also differs from the first in that m = 3 is assumed right from the beginning and the starting approximation is computed by an interpolation to two points of measurement. The actual computation of the best approximation is then carried out using the Harwell V0A04 program, which is an implementation of the variable metrics algorithm.

The solution will be a vector â. In general, â is not equal to a', but â also solves P1 in most instances.

Each test problem was correctly solved by at least one of the two programs. When the programs failed, this failure was apparent so that there was no danger of further operation with erroneous values. The transfer locus found in this way now permits the characteristics of the magnetic field to be computed. For this purpose, a decomposition of the fraction into partial fractions is carried out for the transfer locus:

$$r(a'',x) = A_o + A_1 / (x-\lambda_1) + \dots + A_m / (x-\lambda_m) .$$

This permits a simple interpretation:

The magnetic field in the measuring point is composed of m components $B_1,\dots B_m$ in the steady state, whose amplitudes are proportional to A_k/λ_k and whose response times are given by λ_k.

This interpretation requires the λ_k to be real and positive. Negative or complex λ_k can only arise due to the influence of measuring and rounding errors. In this case, the associated amplitudes are small. The first program provided real positive λ_k values in all cases, but this advantage is obtained at the expense of longer computing times as compared to the second program.

3. Measuring Equipment

H.P. Eulenberg

Extensive hardware and software were required for carrying out the measurements. The software did not only serve to control the operation of automated measurements, but also to process measured signals, which is a task normally performed exclusively by hardware in conventional measuring systems. The measuring equipment therefore consists of hardware and software.

3.1 Measuring equipment hardware

The test van carrying the assembly with the field measuring probes travelled on a circular two-rail configuration through the TEXTOR vacuum vessel (Fig. 16).

The double rail manufactured from synthetical resin-compressed wood (Fig. 2) consisted of a multitude of individual segments bolted to each other and fixed by alignment pins. This type of construction was selected in order to bring the rail into the interior of the TEXTOR vacuum vessel piece by piece through the flanges. The rail featuring a mean diameter of 3.5 m had been worked in one piece on a vertical turning lathe to keep its out-of-roundness as small as possible. An out-of-roundness of 0.02 mm was measured on the outer vertical surface of the rail clamped onto the turning lathe.

Two guide rollers rigidly attached to the test van were running on this rail surface (Fig. 15); these rollers were laterally pressed against the vertical surface of the rail by means of a spring pressure roll in such a way that the test van could be moved on an almost exactly circular path. The rail was supported on and bolted to eight pads extending into the vacuum vessel through the flanges from below. These pads were again supported on the TEXTOR mounting plate. The center of the guide rollers was aligned with the center of the vertical mid-plane of the TEXTOR machine with an accuracy of a few 0.1 mm.

The position of the test van was measured according to the potentiometer method (Fig. 14). For this purpose, two vertical metal strips were inserted into the upper surface of the rail. A stabilized current of approx. 1A flowed through one of these strips. The DC voltage proportional to the conductor length covered by the test van was transmitted to the neighbouring second

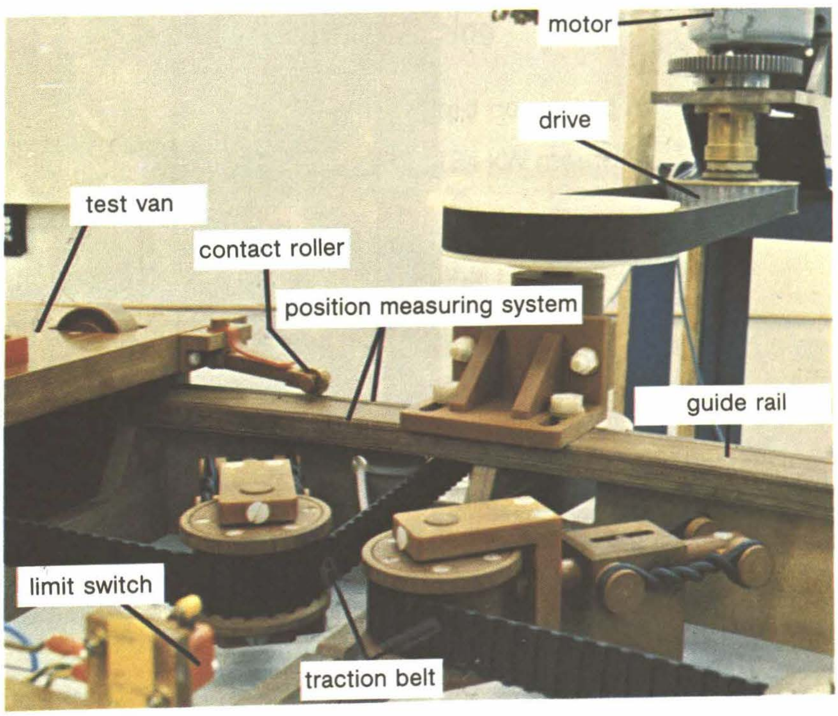

Figure 14
Test van on rails with its traction device and position measuring systems

metal strip via a small wheel attached to the test van, so that the measuring voltage applied at the end could be fed into a six-digit digital voltmeter.

A status signal was generated in a CAMAC* cassette from the target position of the test van preset by the computer program and the actual

2 cm/sec, was then reduced to about 2 mm/sec, so that the test van did not travel beyond the target mark when approaching the position value. This had been a danger because of the relatively large mass of the test van and its field probe holding devices.

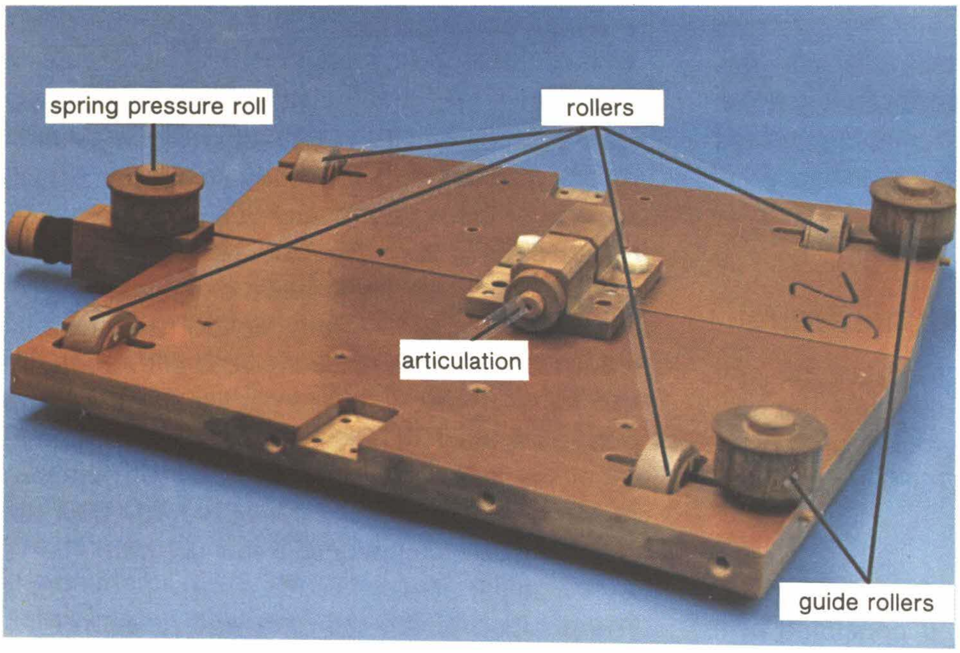

Figure 15
Rollers for moving and guiding the test van on its bottom surface

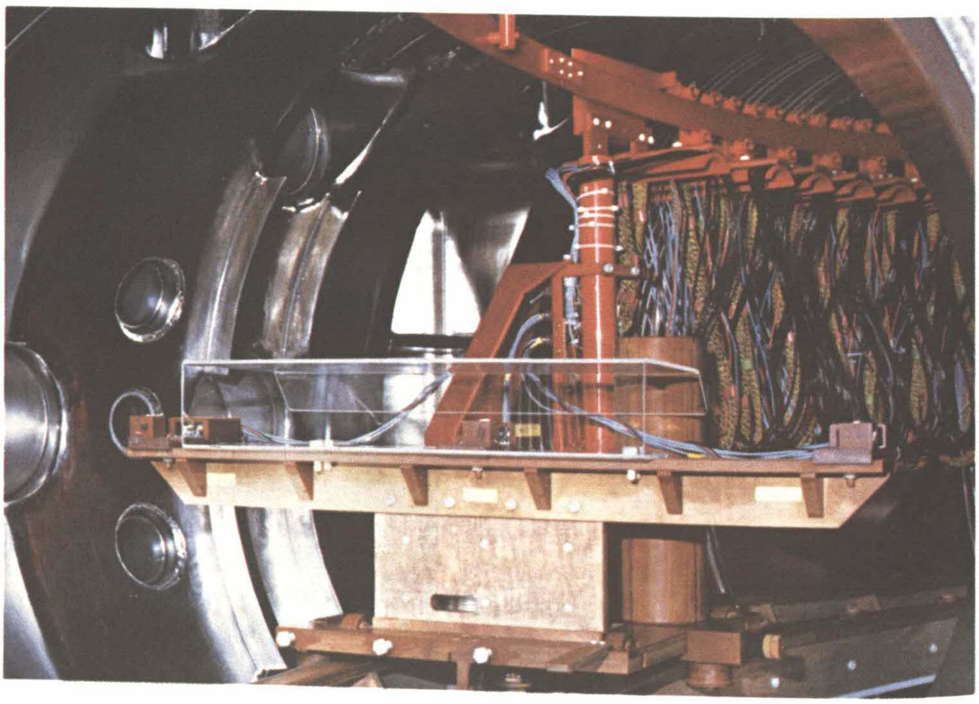

Figure 16
Magnetic field measurement configuration in the interior of the vacuum vessel

position indicated by the digital voltmeter. This signal informed the computer that the test van was about 1 cm in front of the target point. The speed of the test van, which had been approx.

Four different types of measuring probe holding devices were mounted alternatively on the test van, depending on the measuring task. In addition to the Hall field probes, they also carried the amplifiers necessary for amplifying the measuring voltages. Their output voltage was supplied to the measuring rig set up at a distance of

* CAMAC is a modular interface system standardized according to EUR 4100 and independent of the type of computer used

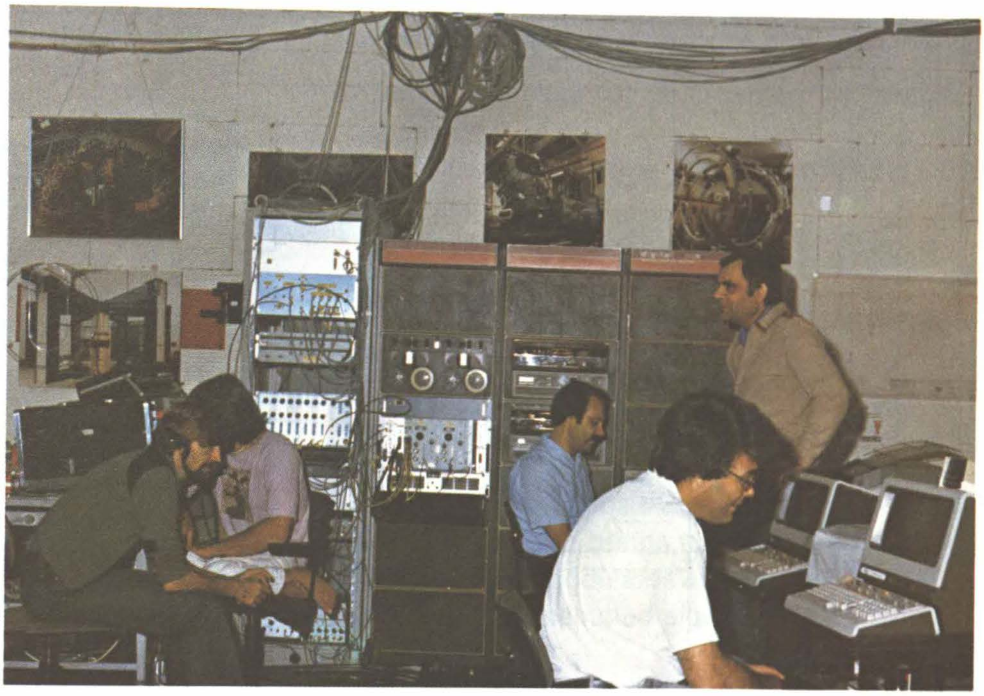

Figure 17
Measuring team in the computerized measuring room

about 10 m from the TEXTOR machine via heavily twisted two-wire lines of approx. 40 m length. The measuring voltage lines as well as the cables required for operating the transmitter-amplifier were tracked in the vacuum vessel by means of a cable transport device attached to the vessel above the double rail (Fig. 16).

As is also shown in Fig. 17, the measuring rig consisted of a PDP-11/40 process computer with CAMAC interface, the measuring electronics and numerous terminals. They were connected to the process computer and the large computer of the KFA. The latter served to monitor the measuring equipment during measurement of the eddy current time constants by computing the entire transfer locus just a few minutes after measurement from the points of the transfer locus of the complex transmission factor ascertained by the process computer, which indicates the influence of the eddy current effects in the frequency range (picture range), and by displaying it on a graphic terminal.

3.2 Measuring equipment software

H. Thyssen

3.2.1 General remarks on data acquisition and processing

The EDP system used consisted of:

a) PDP-11/40 with 124 kW memory,
b) 4 disk drives RK 05,
c) 2 display terminals HP 2640 and 2649, 1 typewriter terminal LA 30,
d) line printer,
e) plotter,
f) 1 CAMAC crate (standard process interface).

The operating system used was RSX-11-M. The software package of the Hahn-Meitner Institute, Berlin, was used for operating the CAMAC crate and all connected process hardware. The driver contained in this package was firmly built into the RSX-11-M operating system upon generation.

The programming language used was FORTRAN IV. Time-critical transfer routines were realized in the MACRO-11 assembler and called up as subroutines of FORTRAN main programs.

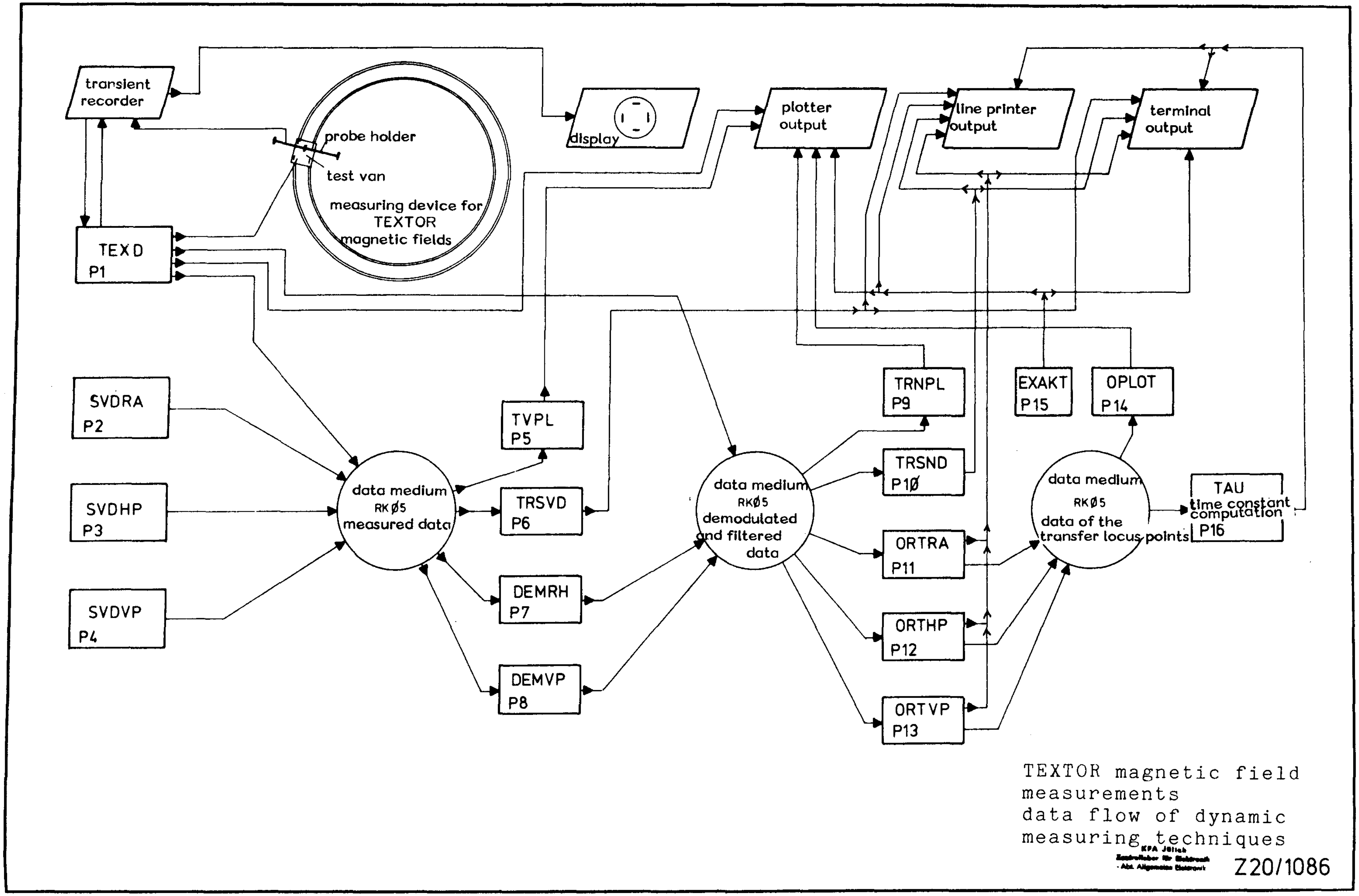

Figure 18
Survey of the measured data acquisition and processing programs and their interaction

The modular programming technique was largely used for the sake of clarity.

This report only describes the main programs.

A detailed program description is given in an internal report[5] of the ZEL.

The memory requirements of the machine code did not exceed the maximum range of 32 kW envisaged in the RSX-11-M system for always 1 main program with associated subroutines.

Only 1 main program, i.e. the program for collecting the data, 'TEXD', was linked in overlay structure because this limit had been exceeded. In this case, only the part of the program just being executed was resident in the memory, while the other program parts were stored externally on the disk and loaded into the memory as required.

There existed two further main programs on the TSS system of IBM 370 for computing the time constants from the transfer locus points. These programs were installed on the large computer at the KFA's computer center because of time-consuming computation. Data transmission from the PDP-11/40 to IBM 370 was effected off-line via a data cartridge which was written by the cartridge drive of an HP terminal connected to the PDP-11.

The cartridge was read in by the cartridge drive of a further HP terminal connected on-line with the IBM. In this way, the data could be further processed in the two programs installed on the IBM:

'TAU1' and 'TAU2' .

3.2.2 Description of the main programs for measuring transient magnetic fields and preparing the data measured

3.2.2.1 *Program TEXD for controlling the measuring apparatus and the acquisition of data*

This program serves to measure the magnetic fields in TEXTOR.

Six modes of operation are distinguished:

a) ramp technique for determining the transfer locus plot, RA
b) half-pulse technique for determining the transfer locus plot, HP
c) full-pulse technique for determining the transfer locus plot, VP
d) field time function with time-dependent constant field, OH
e) demodulator ripple of the toroidal coils, TR
f) demodulator ripple of the vertical coils, VR.

The program positions the test van, operates the transient recorder, brings the measured data onto the disk, demodulates upon request the recorded data of sampled signals.

The output of data of the demodulated sampling sequences is optionally on

a) display
b) plotter
c) RK 05 data medium.

3.2.2.2 Program TVPL for the graphical representation of measured data

This program reads the data off the disk which had been provided either by TEXD or by the simulation programs SVDRA, SVDHP, SVDVP. The data are prepared for plotting and the plotting process is initiated. The program is self-explanatory upon call.

3.2.2.3 Program TRSVD for alphanumeric representation of the measured signal

This program reads the data which had been brought onto the disk (RK05) by either TEXD or the simulation programs SVDRA, SVDHP, SVDVP and issues them as number columns on a random output device such as LP or TI. The header line is also issued and can be used for data identification.

The quantity of data to be issued can be controlled by input parameters.
The program is self-explanatory upon call.

3.2.2.4 Program DEMRH for demodulating the measuring signals generated according to the ramp or half-pulse method

This program demodulates the amplitude-modulated measuring signals generated according to the ramp or half-pulse method and stores the sample results obtained in this way on a disk.

The program can also process the synthetic amplitude-modulated measuring signals generated with the simulation programs SVDRA and SVDHP. The user can control by means of an input parameter whether a 'large' or a 'small' result file is brought onto the disk. A large file means that all the data obtained from the demodulator are brought onto the result file. A small file means that every 8th value obtained in the demodulator is brought onto the result file. (The data are reduced after demodulation.)

The program queries the input parameters upon call. The values in brackets are indicative of the demodulation of a simulated data set generated with the program SVDRA. The results are reduced to 1/8 before being brought onto the disk.

The process for demodulation used in this program is described in detail under item 1.2.

3.2.2.5 Program DEMVP for demodulating the measuring signal generated according to the full-pulse method

This program serves to demodulate the data recorded in the program TEXD as far as these were ascertained using the full-pulse technique (VP) and stored on a disk.

Furthermore, the program furnishes the demodulated measuring signals generated with the simulation program SVDVP.

Only the period measured last is brought onto the disk after demodulation. It is necessary to ensure that the digital filter of the demodulator has assumed its steady state when generating the result data. For this reason, the input data run twice through the filter before the output data are accepted.

After filtering, the length of the period and thus the number of grid points for a period are determined in a subroutine.

The process used in this program for the demodulation of data is described in detail under item 1.2.

3.2.2.6 Program TNPL for the graphical representation of demodulated measuring signals

This program serves for the representation of demodulated data on the Tewidata plotter. The data are prepared, depending on the selected mode of operation, and plotted with the associated coordinate system.

A reduced data set (8 records per channel) is assumed for the modes of operation RA, HP, OH, TR, VR.

A distinction is made between VG (large data set, 64 records per channel) and VK (small data set, 16 records per channel) for the mode of operation VP. Four periods of the full pulse are represented when selecting VG and one period of the full pulse when selecting VK.

3.2.2.7 Program TRSND for alphanumeric representation of the demodulated measuring signal

This program reads the data which had been brought onto the disk by the programs DEMRH and DEMVP and issues them as number columns on a random output device, e.g. line printer or display terminal.

The header line is also issued and can be used for data identification.

The quantity of data to be issued can be controlled by input parameters.

3.2.2.8 Programs ORTRA, ORTHP and ORTVP for determining the complex transmission factor of TEXTOR

These three programs serve for the evaluation of demodulated and possibly reduced data. First of all, the measured ramp is combined to form a complete pulse in the program ORTRA according to the method described in chapter 2.3.1 (RA). The measured half-pulse is complemented in the program ORTHP to form a complete pulse (HP). In the program ORTVP, four complete periods or one complete period are optionally further processed. This is followed in all three programs by a Fourier analysis of the field data measured and a Fourier analysis of the sampling sequence of the excitation current. The real and imaginary parts for each harmonic are divided by each other.

The resultant transfer locus plot points of the complex transmission factor of TEXTOR are then printed out or brought onto the RK05 data medium for further processing or representation.

The algorithm underlying these programs was described in more detail under item 2.3.

3.2.2.9 Program OPLOT for the representation of transfer locus plots

This program reads the data sets provided by the programs ORTRA, ORTHP, ORTVP off the disk. The data are prepared for plotting on the Tewidata plotter and the plotting process is initiated.

The program is self-explanatory upon call.

3.2.2.10 Programs TAU1 and TAU2 for time constant computation from the complex transmission factor of TEXTOR

These programs read data, which are on an IBM VS data set and contain the transfer locus plot points as well as further identification parameters, and compute from these the time constants of the eddy current effects.

Upon request, the transfer locus is plotted and a document with the results provided on the line printer.

The programs TAU1 and TAU2 differ by the type of algorithms used and can be used alternatively; they should provide equal results.

The results can differ, however, in the case of extremely disturbed input data sets. A meaningful selection of the correct transfer locus plot can be made in such cases by considering the plot.

These programs run on the TSS system of the IBM 370. The algorithm used is explained in detail under item 2.4.

3.2.3 Programs for the generation of test functions

3.2.3.1 Program EXACT for computing and representing the theoretical transmission function of TEXTOR

The resultant transfer locus points are issued numerically on the line printer. On request, the points are additionally brought onto the Tewidata plotter. Plotting is made without coordinate system in this case.

This serves for comparing a plot of the measured transfer locus points by superplotting with the theoretical points using the program ORTPLO.

The program is self-explanatory.

3.2.3.2 Programs SVDRA and SVDHP for testing the software used for the ramp and half-pulse methods

These programs serve to simulate the data furnished by TEXTOR and measured according to the ramp method (half-pulse method), RA (HP). The file established corresponds in its size and contents to the data file produced by the program TEXD and serves to verify the evaluation software based on this measuring technique:

FILTRH and ORTRA (ORTHP).

3.2.3.3 Program SVDVP for testing the software used for the full-pulse method

The program serves to simulate the data furnished by TEXTOR and measured according to the full-pulse method (VP).

The file established corresponds in its size and contents to the data files produced by the program TEXD and serves to verify the evaluation software based on this measuring technique:

DEMVP , FILTVP and ORTVP .

The Measurements and their Results

Hp. Eulenberg
H. Thyssen

4. Measurements

Measurements of the transient magnetic fields in TEXTOR were carried out using the field probe holding devices made of laminated fabric as shown in Figures 19 and 20. Both the horizontal field probe holder shown in Figure 19 and the vertical field probe holder of Figure 20 were mounted alternatively onto the test van, depending on the measuring task. Three field probes of the type described in chapter 2.1 and shown in Figure 3 were arranged horizontally at a distance of 470 mm on the horizontal field probe holder. The distance between the field probes on the vertical field probe holder was 200 mm. The field probes seated in the center of each of the two holding devices always moved in the mid-plane of the TEXTOR vacuum vessel on the so-called 'mid-radius' R_o when the test van was running on the rail.

The field probes were aligned in such a way that the vertical component of the magnetic induction and the component pointing radially to the center of the TEXTOR machine were measured on both field probe holding devices.

The measuring voltages of the field probes changing in the course of time were given for storage to the channels 1 - 6 of the transient recorder shown in Figure 21. The allocation of its

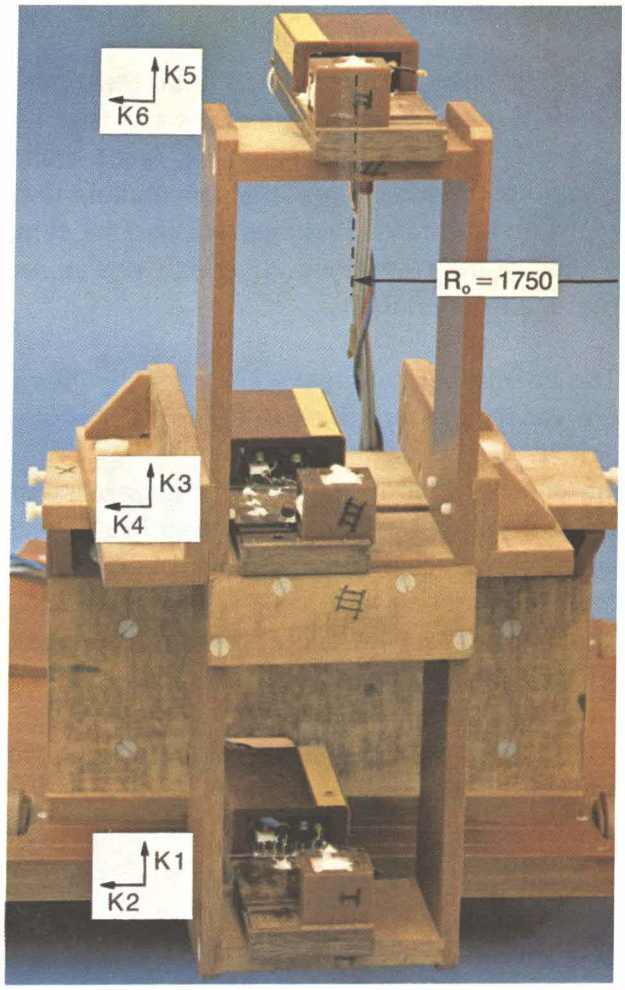

Figure 20
Vertical field probe holder

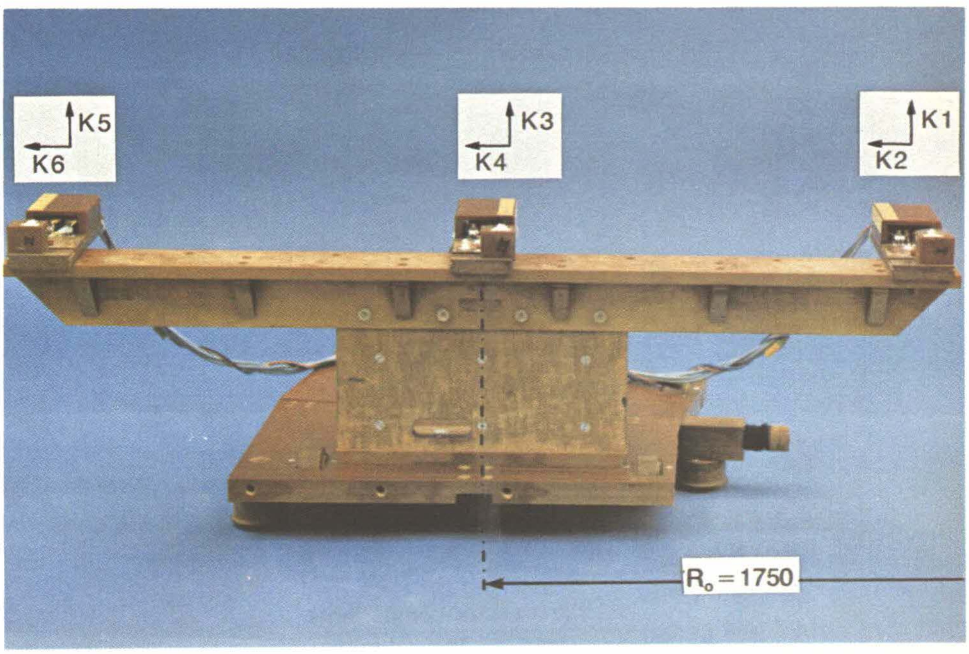

Figure 19
Horizontal field probe holder

channels to the respective induction components can be seen in Figures 19 and 20 as well as the identifications appearing on the measurement printouts.

It should also be mentioned that the time-dependent measuring voltage of the excitation current of the respective magnetic fields was recorded by channel 7 and that the sample results of the 10 kHz carrier voltage required for demodulation of the measuring voltages were stored in the eighth channel.

The position of the test van in the TEXTOR vacuum vessel was specified in degrees of angle.

As can be seen in Figure 22, the zero position angle (toroidal angle) was placed in the middle of the toroidal field coil 3. The position of the bellows connecting the thick-walled parts of the vacuum vessel with each other and the position of the vessel flanges are also entered in this general drawing, so that their influence can be quickly recognized when interpreting the measuring results.

4.1 Measurement of the vertical component of the magnetic field in the ignition phase

Since no magnetic confinement is realized yet in the ignition phase of TEXTOR, vertical components of the magnetic induction lead to undesired transversal drift motions on the already existing charge carriers due to the Lorentz force, which counteract plasma formation. In order to keep the carrier losses low, the vertical component in TEXTOR should not be greater than 2 mT to 3 mT in the ignition phase[2].

The task in measuring the vertical component of the magnetic field therefore consisted in measuring its time dependence from the moment of reaching the loop voltage required for ionization in different points of the vessel cross section and in the toroidal direction.

The sampling process in seven channels of the transient recorder was triggered by means of a trigger pulse derived from the control of the magnetizing circuit. The six measuring signals of the field probes which were amplitude-modulated via the drive current of the Hall field probes were sampled in the transient recorder with a sampling frequency of 250 kHz, digitized and stored. The time-dependent course of four signals demodulated in the process computer in the way described in chapter 2.2 is shown in Figure 23 and Figure 25.

The induction time functions shown in Figure 23, which were determined in the test van positions 0° and 11.25°, were measured with the vertical field probe holder. Three curves can be seen in each of the two diagrams. They were measured with the Hall field probes K1, K3 and K5. The probe K5 at the top of the vertical holder indicat-

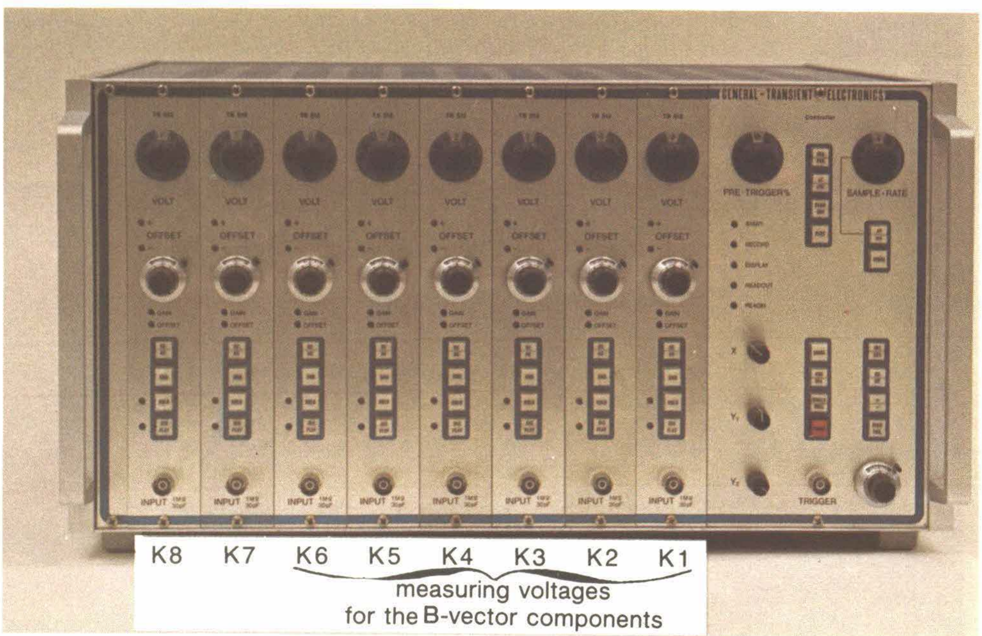

Figure 21
Eight-channel transient recorder used for converting the time-dependent measuring voltages into numerical measured value sequences

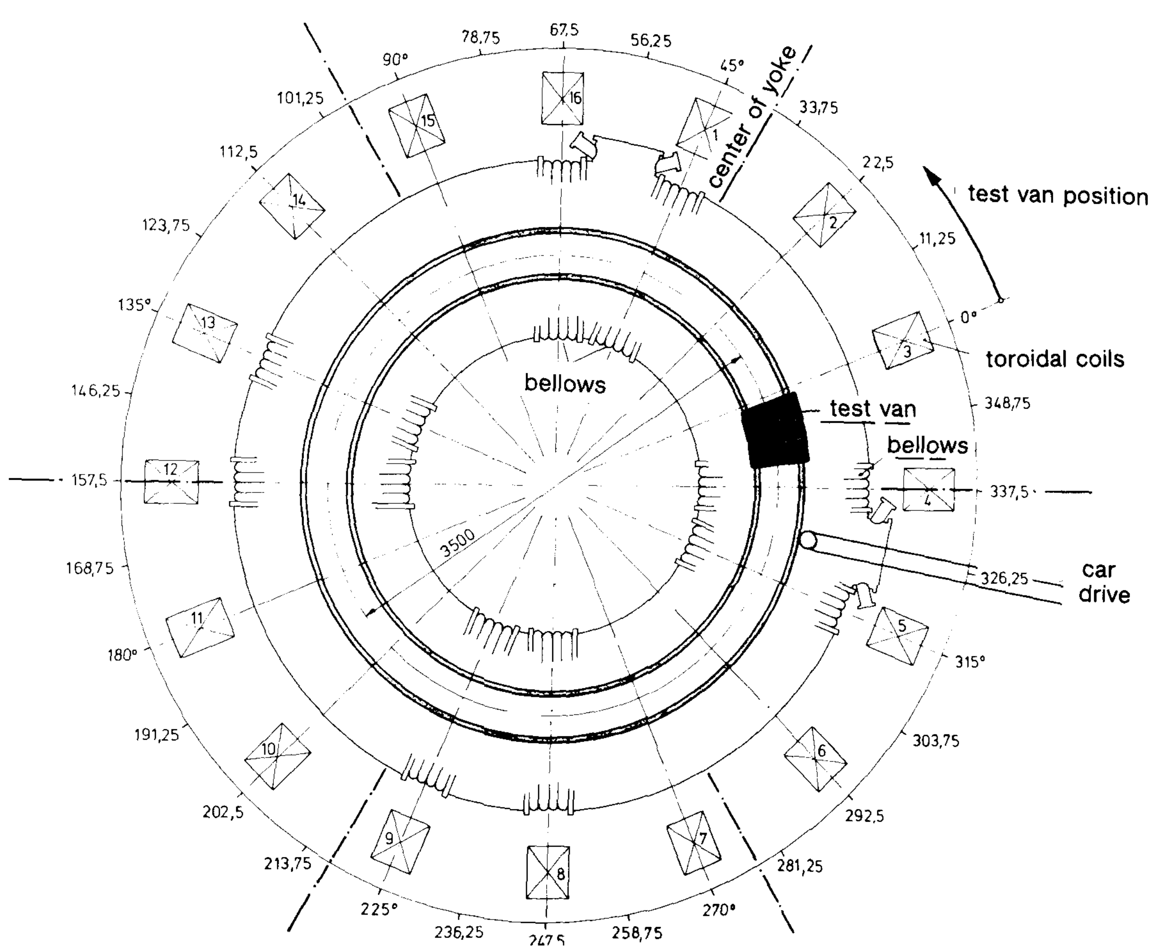

Figure 22
Position of the measuring rail and test van in the vacuum vessel of TEXTOR

ed the largest maximum value for all measurements carried out in 29 measuring planes evenly distributed over the machine periphery, whereas the probe K1 arranged at the bottom showed the smallest value. The measured curves to be seen in the upper half of Figure 23 only insignificantly exceed the preset limit of 2 mT to 3 mT. The maximum values of each individual field time function measured in 29 measuring planes with measuring channel 5 at 51 % excitation current are plotted in Figure 24 over the machine periphery.

Measurements carried out with and without a bank of capacitors and with 100 % excitation current in five measuring planes using the horizontal field probe holder provided the induction time functions shown in Figure 25 for the test van positions 0° and 11.26°.

The charge stored in the bank of capacitors serves to enhance the time-dependent magnetic field rise in order to increase the loop voltage in the plasma.

4.2 Measurement of the eddy current time constants of the vertical field

Measurements were carried out in three test van positions underneath a bellows and underneath a solid section of the vacuum vessel.

These measurements were carried out in the field of the vertical coil using the horizontal field

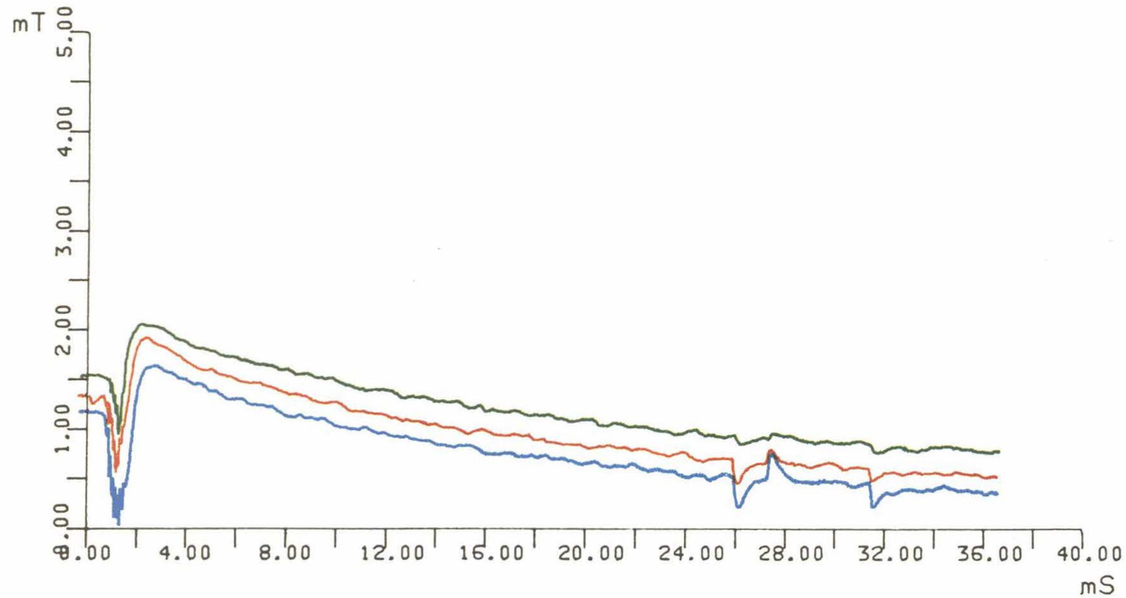

Field Measurement on the BM System
without bank of capacitors

date	=	30-JUL-81
time	=	09:40:44
data medium/data set	=	DAT1/M1.BM2
measuring position(degrees)	=	0.00
probe	=	vertical holder
field direction	=	vertical
current (amps.) 50 %	=	1850
max.value channel 1 (mT)	=	1.66
max.value channel 3 (mT)	=	1.94
max.value channel 5 (mT)	=	2.10

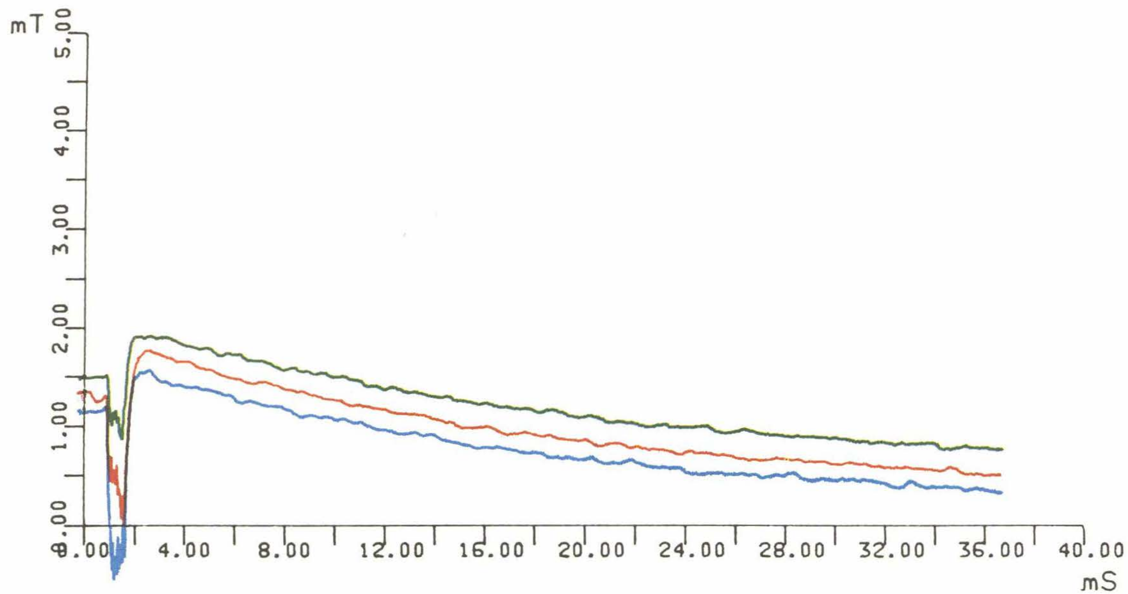

Field Measurement on the BM System
without bank of capacitors

date	=	30-JUL-81
time	=	09:45:43
data medium/data set	=	DAT1/M2.BM2
measuring position(degrees)	=	11.26
probe	=	vertical holder
field direction	=	vertical
current (amps.) 50 %	=	1850
max.value channel 1	=	1.59
max.value channel 3	=	1.79
max.value channel 5	=	1.96

Figure 23

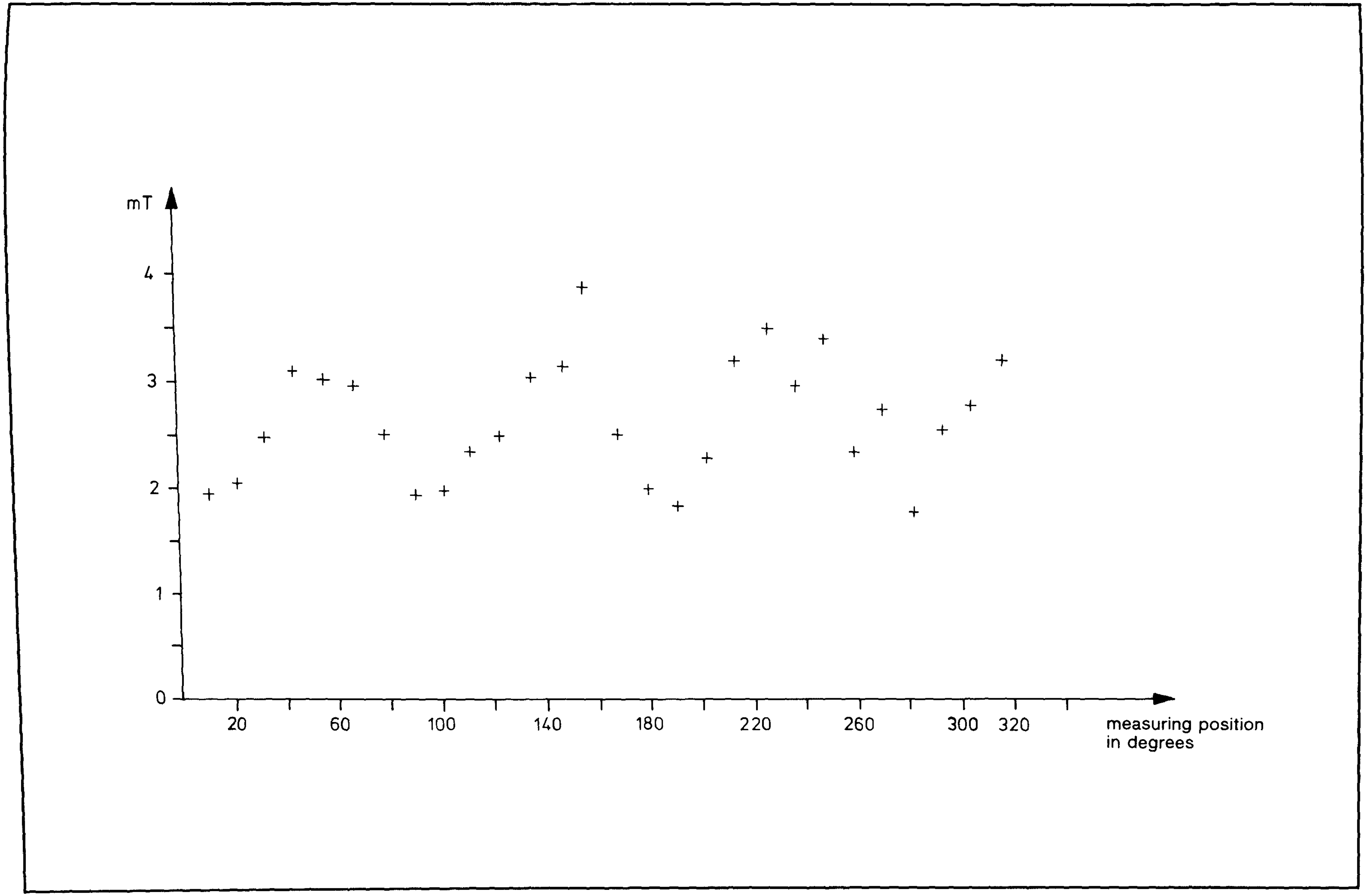

Figure 24

Dependence of the maximum vertical field of channel 5; vertical holder at 50% excitation current

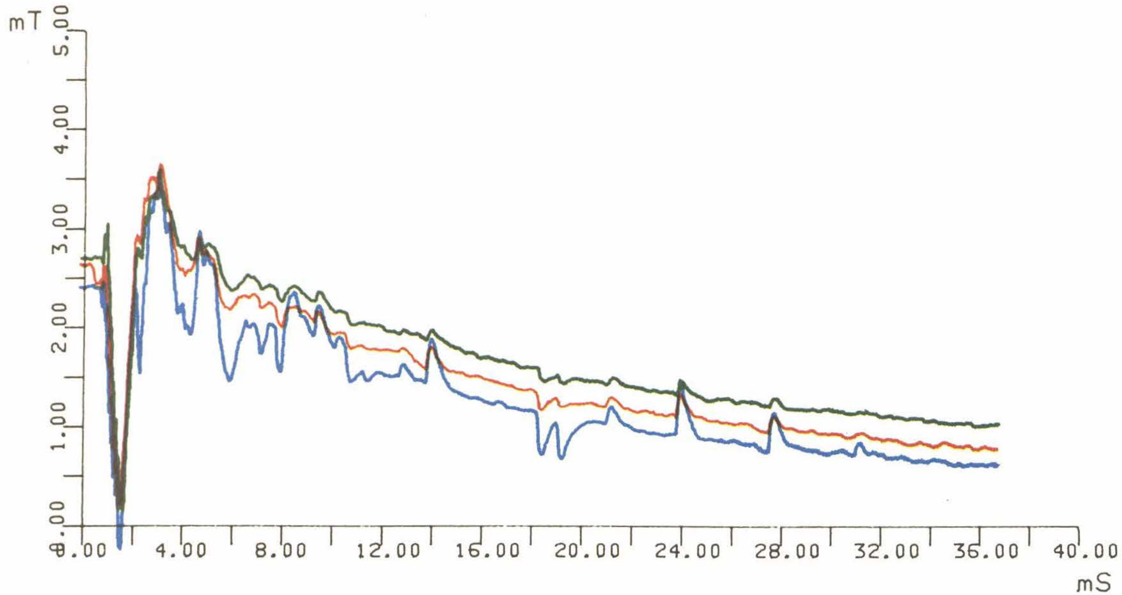

Field Measurement on the BM System
without bank of capacitors

date	=	30-JUL-81
time	=	14:09:22
data medium/data set	=	DAT3/M1.BM1
measuring position(degrees)	=	0.00
probe	=	vertical holder
field direction	=	vertical
current (amps.) 100 %	=	3605
max.value channel 1 (mT)	=	3.59
max.value channel 3 (mT)	=	3.64
max.value channel 5 (mT)	=	3.44

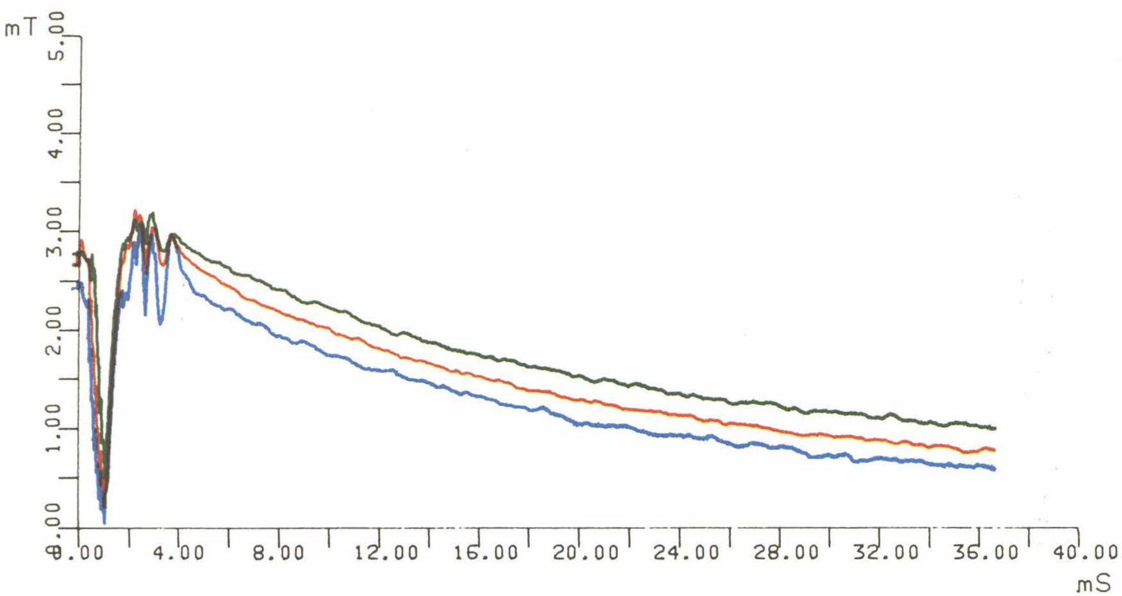

Field Measurement on the BM System
without bank of capacitors

date	=	30-JUL-81
time	=	14:16:49
data medium/data set	=	DAT3/M2.BM1
measuring position(degrees)	=	11.26
probe	=	vertical holder
field direction	=	vertical
current (amps.) 100 %	=	3605
max.value channel 1 (mT)	=	3.06
max.value channel 3 (mT)	=	3.21
max.value channel 5 (mT)	=	3.19

Figure 25

probe holder (Figure 19). This field constitutes the poloidal field of TEXTOR together with the field of the plasma.

First of all, the complex transmission factor defined according to eq. 2.3.2-4 was measured by means of the ramp technique described in chapter 2.3.1 from the magnetic field rise caused by the time-proportional excitation current when turning on the vertical coils. This transmission factor was graphically represented as a transfer locus in the complex plane. As already described in detail in chapter 2.3, it contains the time constants with which the eddy currents flowing in the metal parts of the machine and the magnetic fields produced by them are exponentially decaying. The time constants were computed according to the method described in chapter 2.4 using the measured points of the transfer locus.

Two of the total number of nine normalized transfer loci measured are shown as an example in Fig. 26 and Fig. 27. The transfer locus in Fig. 26 was measured in the test van position 11.24°, i.e. underneath a thick-walled part of the vacuum vessel (see Figure 22).

In this case, the influence of the eddy current fields is rather high, as is also clearly indicated by the transfer locus intersecting the real axis at approx. 0.1. The transfer locus shown in Fig. 27 gives a different picture. In this case, the eddy current effect underneath the bellows is clearly smaller, since the real axis is intersected at 0.67.

Two time constants could be measured underneath a solid section of the vacuum vessel using the ramp technique. One of them is 9.13 msec, the other 30.53 msec. Underneath the bellows, only the larger time constant could be ascertained which was 11.13 msec in the test van position 45.04°.

4.3 Measurement of the eddy current time constants in the magnetic field of the coils K_z and K_r for plasma position control

The fields of the coils K_z and K_r in TEXTOR have the task of adjusting the plasma ring in the radial and vertical direction in the phase of plasma generation by means of a control device in such a way that it can always be kept away from the migrations of the liner built into the vacuum vessel [3]. The two field excitation currents are produced in a 4-quadrant regulating unit [4]. Since the fields are to act as quickly as possible on the plasma ring through the metallic vacuum vessel and the liner, in order to readjust the position of the plasma ring as quickly as possible, those field fractions impeding the direct field interference, which are caused by the eddy currents in the metallic vessels, must decay with sufficiently small time constants. The measuring task was to measure the unit envisaged for operation of the plasma position control.

For this purpose, the field probes had been mounted again onto the horizontal field probe holder (Figure 19). The transfer loci reflecting the influence of the eddy current effects were measured in 29 measuring planes distributed over the periphery of TEXTOR, i.e. in 29 test van positions. They were determined according to the full-pulse method described in chapter 2.3.1. The periodic excitation current for the coils K_z and K_r required for this purpose was generated in the 4-quadrant regulating unit by alternating application of positive and negative DC voltages on the coils so as to produce periodic, exponentially obliterated triangular currents. The repetition frequency for the excitation current of the K_z and K_r coils was approx. 25 Hz. Due to the large time constants as compared to the period of the excitation currents and because of the low-pass filtering effect of the metallic vacuum vessel, the harmonics of the periodic field strength time signal were suppressed to such an extent that only its fundamental wave could be used for transfer locus determination. This means that the normalized transfer locus could only be determined by one measuring point and, consequently, only one eddy current time constant could be ascertained.

These restrictions did not apply to the eddy current time constant measurements on the vertical field - chapter 3.2. Two measuring points would have been necessary there for determining a second-degree transfer locus (two time constants), but two additional measuring points were to be found on the approximated solid transfer locus.

Figures 28 to 31 again show the influence of the solid sections of the vacuum vessel and of the bellows on the diameter of the transfer loci and, consequently, the influence of the eddy current fields on the field in the measuring point for both the fields of the coil K_z and those of the coil K_r.

FIELD MEASUREMENT BV

NORMALIZED TRANSFER LOCUS

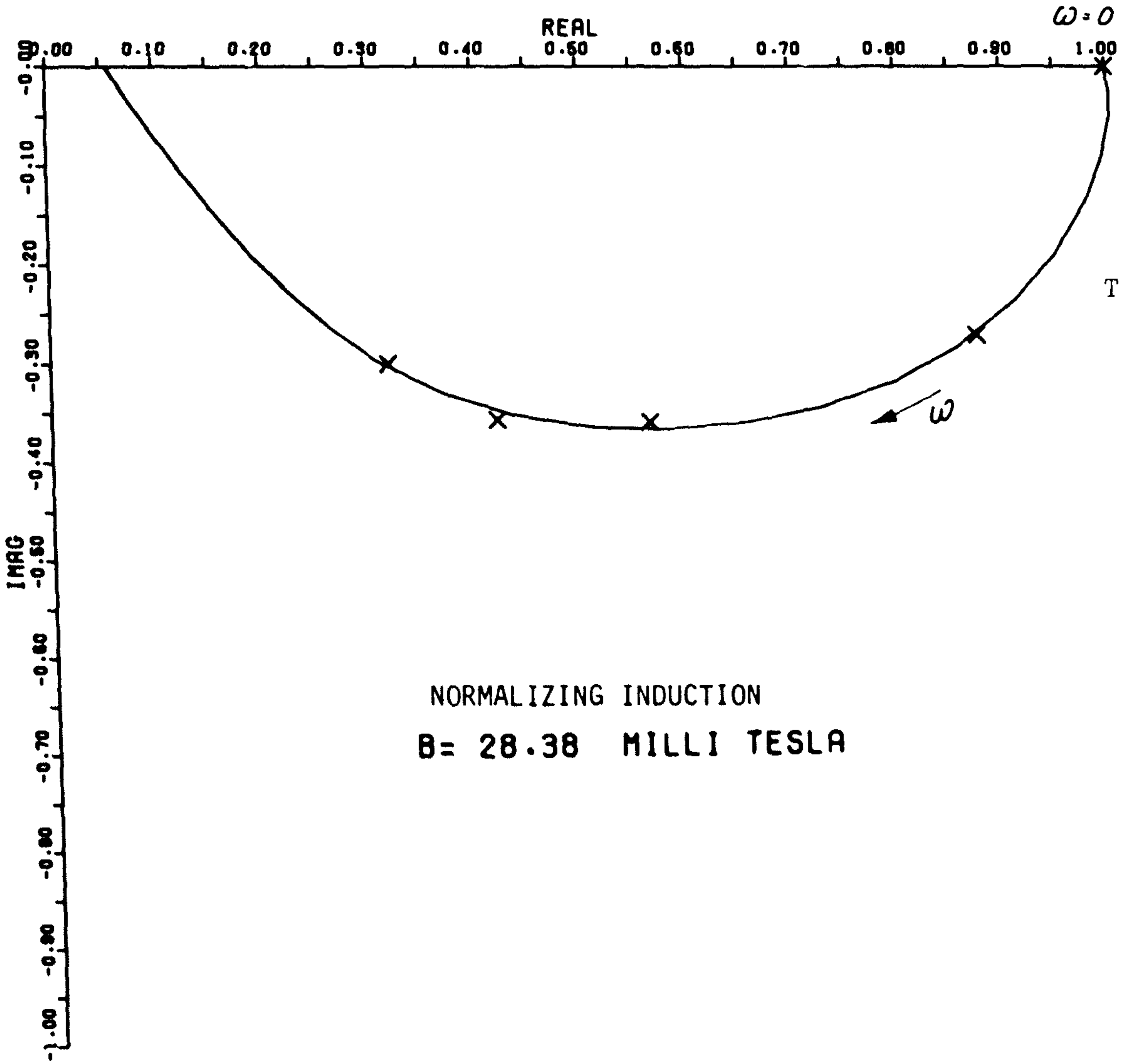

PROBE 3

DATE 05-AUG-81

TIME 09:27:41

TYPE OF MEASUREMENT RA

TEST VAN POSITION (DEGREE) 11.24

GRID POINTS
PER PERIOD 29441

LENGTH OF PERIOD (MS) 294.40

CURRENT (A) 7500.0

DATA MEDIUM/
DATA SET DAT10/M1.RA4

REL. AMPLITUDE OF THE E-FUNCTION

A= -0.40

TIME CONSTANT

TAU= 30.53 MS

REL. AMPLITUDE OF THE 2ND E-FUNCTION

A2= -0.46

2ND TIME CONSTANT

TAU2= 9.13 MS

Figure 26

FIELD MEASUREMENT BV

NORMALIZED TRANSFER LOCUS

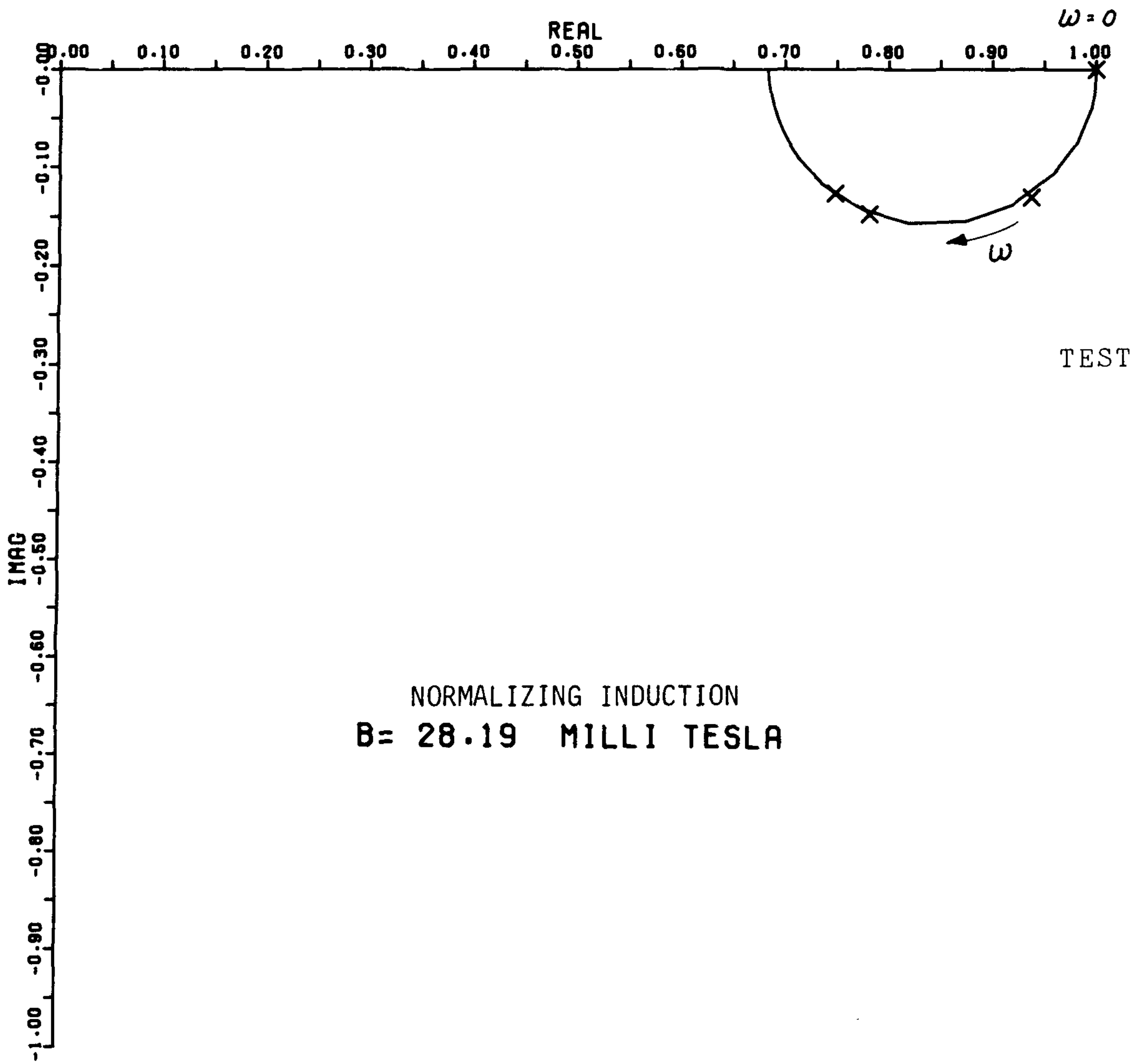

NORMALIZING INDUCTION
B= 28.19 MILLI TESLA

PROBE	3
DATE	05-AUG-81
TIME	09:34:12
TYPE OF MEASUREMENT	RA
TEST VAN. POSITION (DEGREE)	45.04
GRID POINTS PER PERIOD	29441
LENGTH OF PERIOD (MS)	294.40
CURRENT (A)	7500.0
DATA MEDIUM/ DATA SET	DAT10/M2.RA4

REL. AMPLITUDE OF THE E-FUNCTION
A= -0.32

TIME CONSTANT
TAU= 22.13 MS

Figure 27

FIELD MEASUREMENT BV

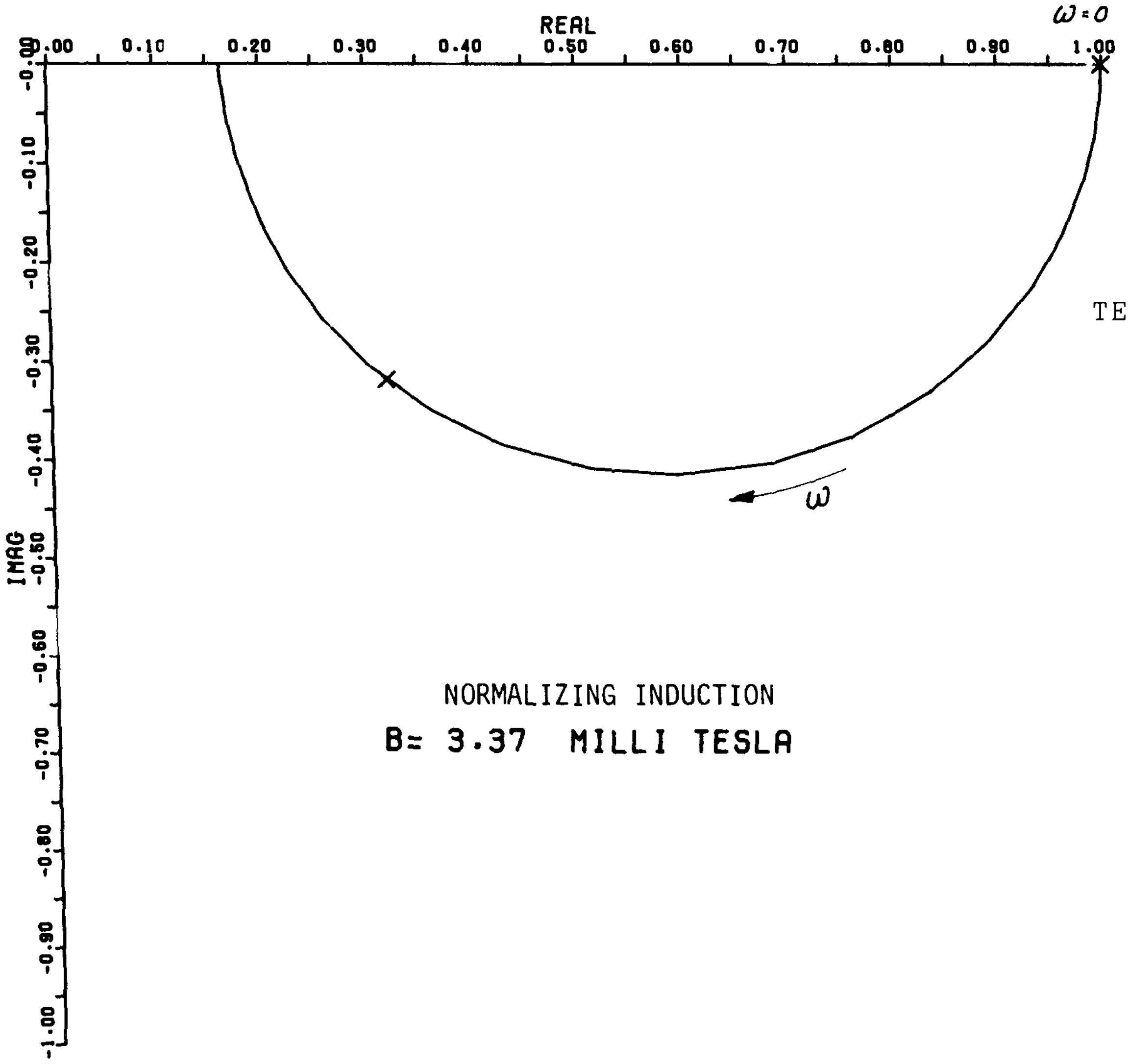

NORMALIZING INDUCTION

B= 3.37 MILLI TESLA

NORMALIZED TRANSFER LOCUS

PROBE	3
DATE	31-JUL-81
TIME	14:12:36
TYPE OF MEASUREMENT	VP
TEST VAN POSITION (DEGREE)	11.27
GRID POINTS PER PERIOD	2001
LENGTH OF PERIOD (MS)	40.02
CURRENT (A)	2600.0
DATA MEDIUM/ DATA SET	DAT5/M3N1.KZ

REL. AMPLITUDE OF THE E-FUNCTION

A= -0.83

TIME CONSTANT

TAU= 13.63 MS

Figure 28

FIELD MEASUREMENT BV

NORMALIZED TRANSFER LOCUS

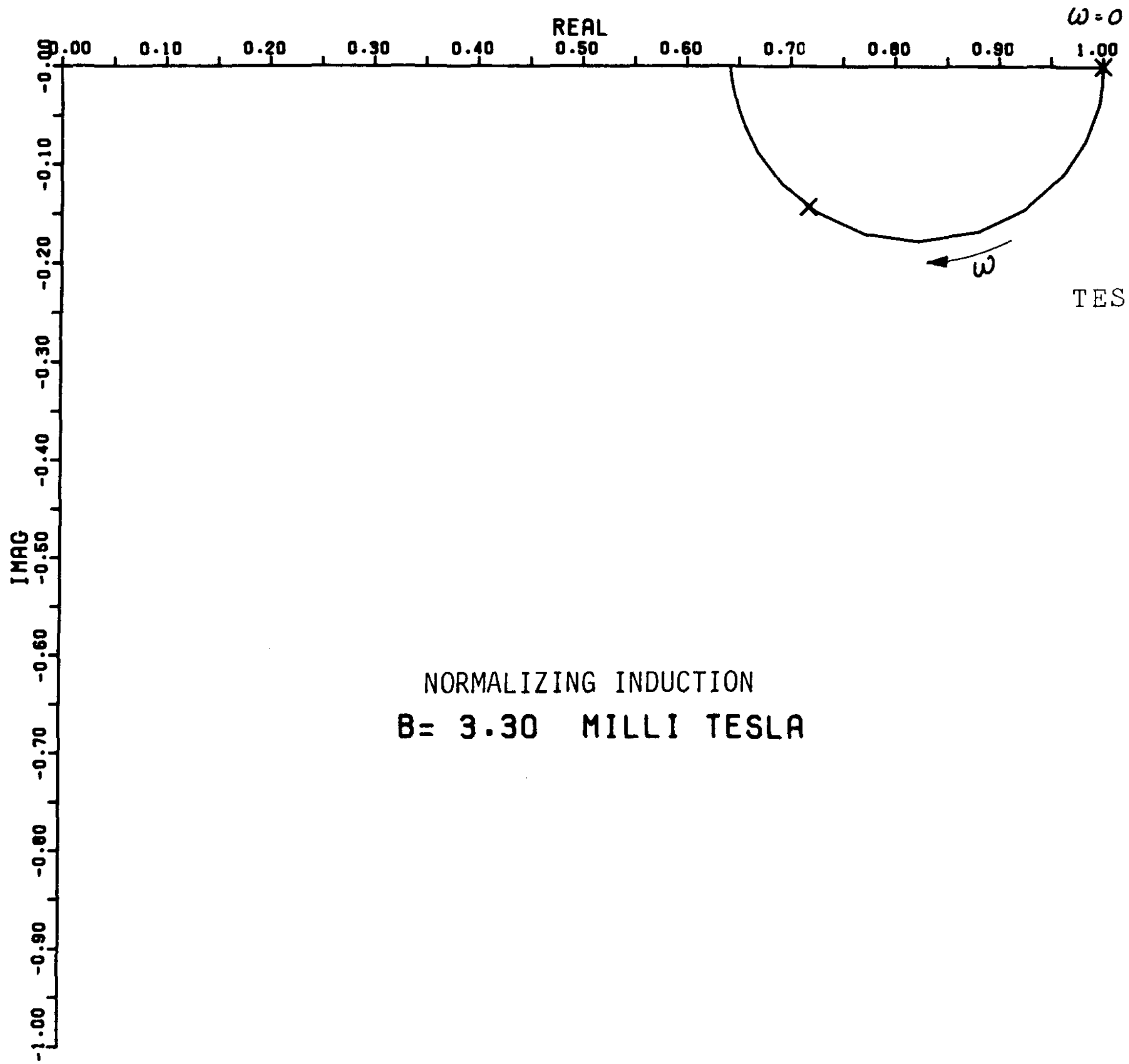

PROBE	3
DATE	31-JUL-81
TIME	15:08:01
TYPE OF MEASUREMENT	VP
TEST VAN. POSITION (DEGREE)	45.03
GRID POINTS PER PERIOD	2001
LENGTH OF PERIOD (MS)	40.02
CURRENT (A)	2600.0
DATA MEDIUM/ DATA SET	DAT6/M9N1.KZ

REL. AMPLITUDE OF THE E-FUNCTION

A= -0.36

TIME CONSTANT

TAU= 12.68 MS

Figure 29

FIELD MEASUREMENT BV

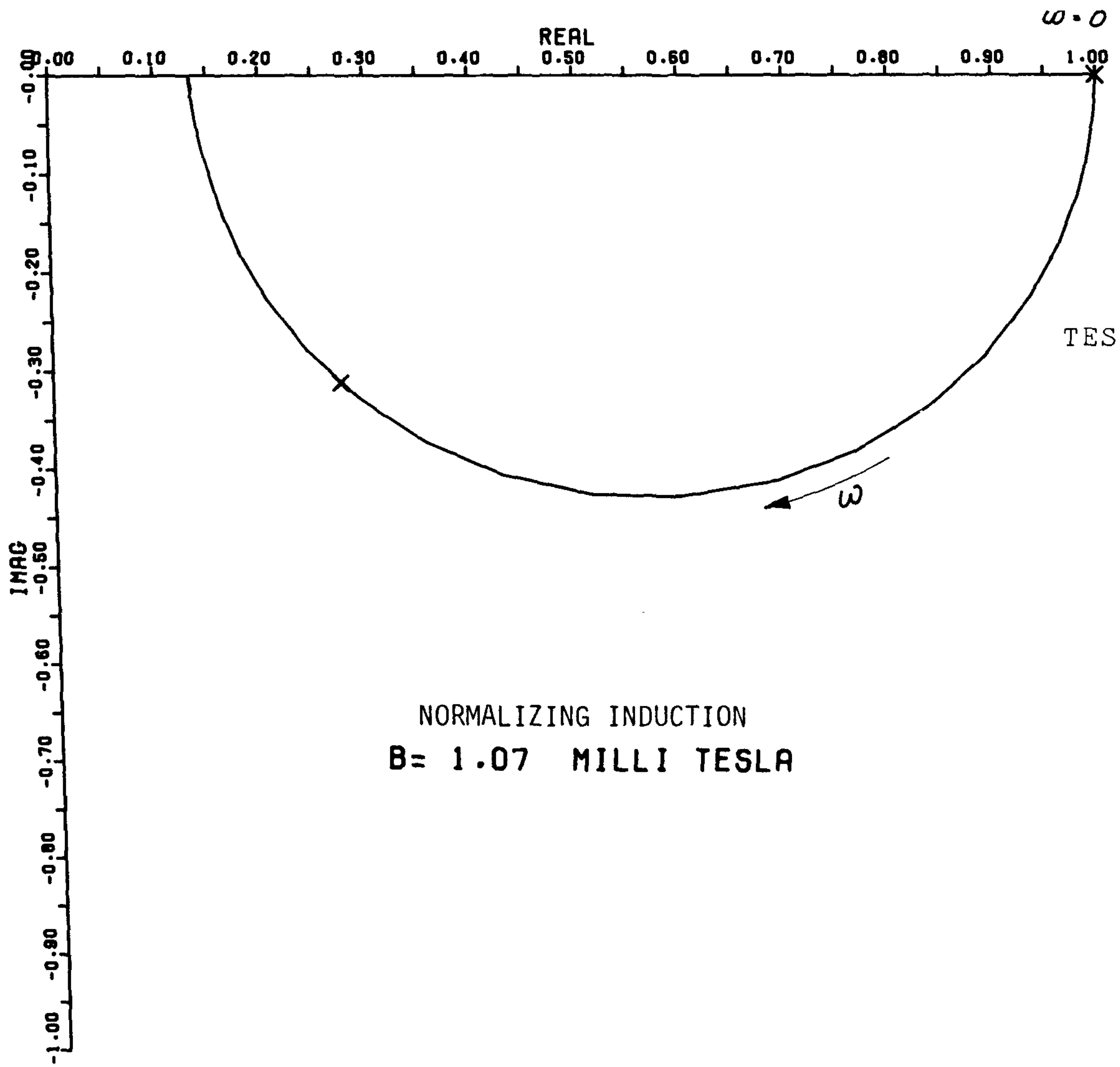

NORMALIZING INDUCTION
B= 1.07 MILLI TESLA

NORMALIZED TRANSFER LOCUS

PROBE	4
DATE	05-AUG-81
TIME	10:34:46
TYPE OF MEASUREMENT	VP
TEST VAN POSITION (DEGREE)	11.25
GRID POINTS PER PERIOD	2001
LENGTH OF PERIOD (MS)	40.02
CURRENT (A)	750.0
DATA MEDIUM/ DATA SET	DAT10/M2N1.KR

REL. AMPLITUDE OF THE E-FUNCTION
A= -0.86

TIME CONSTANT
TAU= 14.82 MS

Figure 30

FIELD MEASUREMENT BV

NORMALIZED TRANSFER LOCUS

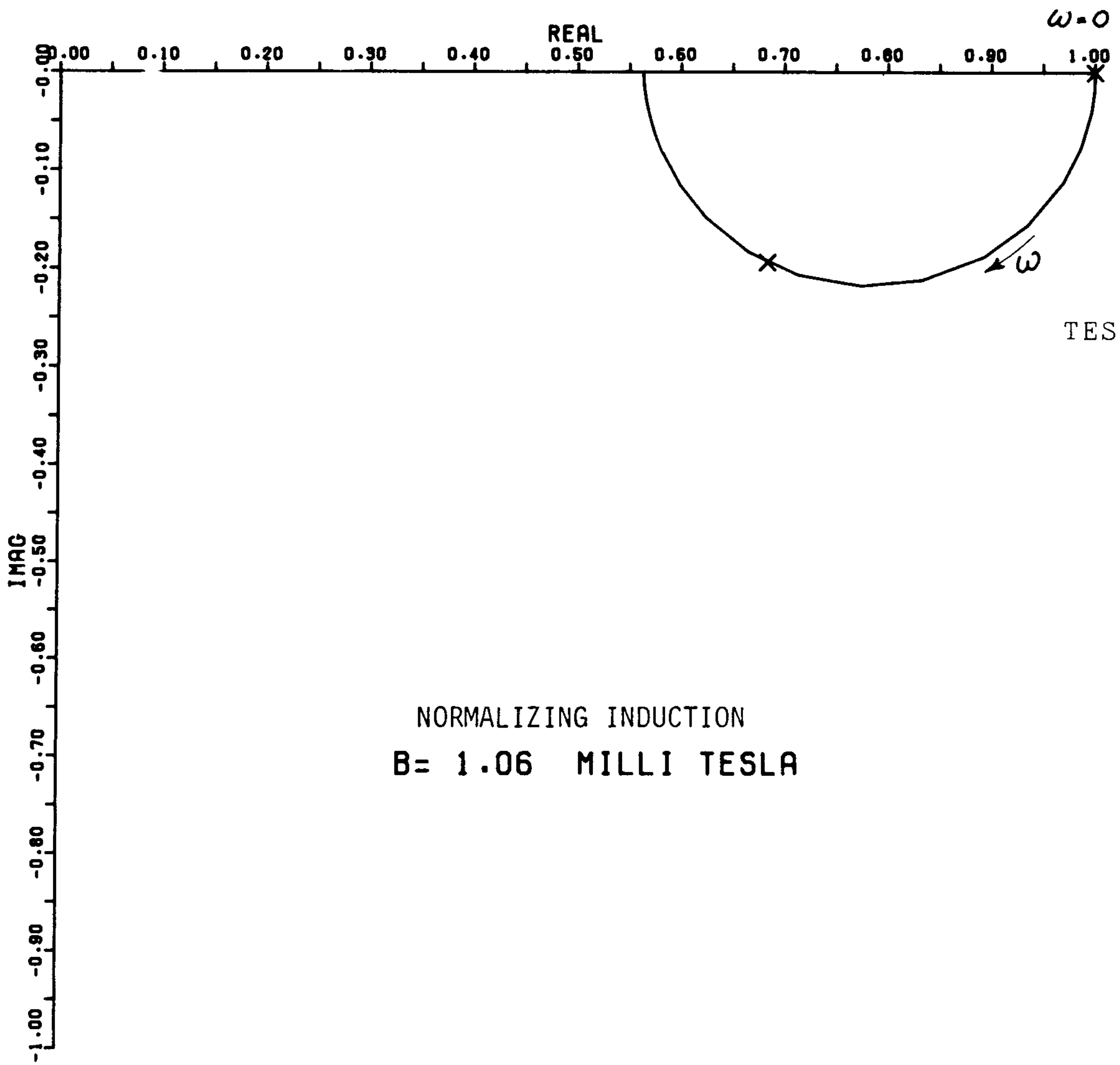

PROBE	4
DATE	05-AUG-81
TIME	11:06:53
TYPE OF MEASUREMENT	VP
TEST VAN POSITION (DEGREE)	56.25
GRID POINTS PER PERIOD	2001
LENGTH OF PERIOD (MS)	40.02
CURRENT (A)	750.0
DATA MEDIUM/ DATA SET	DAT11/M6N1.KR

NORMALIZING INDUCTION

B= 1.06 MILLI TESLA

REL. AMPLITUDE OF THE E-FUNCTION

A= -0.43

TIME CONSTANT

TAU= 10.45 MS

Figure 31

Literature

[1] Hp. Eulenberg
Eine Methode zur Simulation der Bewegung elektrisch geladener Elementarteilchen im Magnetfeld
Reports of the Jülich Nuclear Research Center,
JÜL-1594, pp. 21-29

[2] G. Waidmann
Zur Zündphase einer Tokamakentladung
Reports of the Jülich Nuclear Research Center,
JÜL-1467

[3] W.A. Brocke, G. Waidmann
Measurement and Dynamic Control of Plasma Position in TEXTOR
12th Symp. on Fusion Technology 1982

[4] A. Seeger, W. Schalt
A Fast Response Unit for Vertical Plasma Position Control in TEXTOR
Contributions to 10th SOFT, Padua 1978

[5] G. Breuer, Hp. Eulenberg, U. Sieling, H. Thyssen
TEXTOR Magnetfeld-Messungen
Internal Report KFA/ZEL, No. 5001081